https://doi.org/10.5194/bg-2019-325
Preprint. Discussion started: 26 August 2019
© Author(s) 2019. CC BY 4.0 License.

Biogeosciences Discussions

High resolution ^{14}C bomb-peak dating and climate response analyses of subseasonal stable isotope signals in wood of the African baobab – A case study from Oman

Franziska Slotta[1,2], Lukas Wacker[3], Frank Riedel[1], Karl-Uwe Heußner[4], Kai Hartmann[1], and Gerhard Helle[1,2]

[1] Freie Universität Berlin, Institute of Geological Sciences, Berlin, Germany
[2] GFZ German Research Centre for Geosciences, Section 4.3 Climate Dynamics and Landscape Evolution, Potsdam, Germany
[3] ETH Zürich, Laboratory of Ion Beam Physics, Zürich, Switzerland
[4] Deutsches Archäologisches Institut, Scientific Department of the Head Office, Berlin, Germany

Correspondence to: Gerhard Helle, ghelle@gfz-potsdam.de and Lukas Wacker, wacker@phys.ethz.ch

Abstract. The African baobab, *Adansonia digitata*, has great paleoclimatological potential because of its wide distributional range and millennial lifespan. However, dendroclimatological approaches are hampered by dating uncertainties due to its parenchyma-dominated wood anatomy. Here, securely-dated time series of annual wood increment growth and intra-ring stable isotopes of carbon and oxygen of cellulose for a baobab tree from Oman covering 1941 to 2005 were established. Precise dating with the bomb peak by highly resolved ^{14}C measurements proved the annual character of the baobab's growth rings. But, $F^{14}C$ values of tree-ring cellulose were found up to 8.8 % lower than in the corresponding atmospheric CO_2 for the period around the bomb peak. In conjunction with a considerable autocorrelation of the $\delta^{13}C$ series this points to the incorporation of previous years` carbon significantly affecting the average age of derived wood. Terminal parenchyma bands, marking the tree-ring boundaries, were found to be significantly younger than their corresponding tree ring indicating that parenchyma tissue is alive for many years undergoing cell division, reorganization and potential growth. No autocorrelation was found in the $\delta^{18}O$ series of tree-ring cellulose despite the huge water-storage potential of this stem-succulent tree species. Tree-ring width and stable isotope ratios have revealed significant climate sensitivity. $\delta^{18}O$ was found to be a good climate proxy followed by tree-ring width and $\delta^{13}C$. Tree-ring width and intra-ring $\delta^{18}O_{min}$ correlated well with each other and with precipitation amount for the period from pre-monsoon May to the end of the monsoon season in September/October. Intra-annual stable isotope courses were found rather similar for both $\delta^{13}C$ and $\delta^{18}O$. Years with particularly low monsoon rain were reflected by increased stable isotope values in the mid-section of intra-annual courses. Distinct patterns with low subseasonal isotope values seem indicative for years with heavy rainfall events from pre-monsoonal cyclones. Rain events from post-monsoonal cyclones may also be recorded, however, only two years of observation prevent from a conclusive evaluation.

https://doi.org/10.5194/bg-2019-325
Preprint. Discussion started: 26 August 2019
© Author(s) 2019. CC BY 4.0 License.

Biogeosciences Discussions Open Access EGU

1 Introduction

The African baobab, *Adansonia digitata*, has aroused growing interest for its widespread distribution and longevity promising large paleoclimatological potential. As revealed by radiocarbon dating, individuals can reach ages of 1,000 up to 2,500 years (Swart, 1963; Riedel et al., 2014; Patrut et al., 2017, 2018;). Radiocarbon dating has not just helped to reveal baobabs being the longest-living angiosperm tree species on earth, but also resolved specific multi-stem tree structures of the biggest, monumental individuals in Africa (Patrut et al., 2015a,b, 2017, 2018). The species inhabits (semi-)arid areas across the African continent and the south-eastern Arabian Peninsula (Wickens, 1979; Wickens and Lowe, 2008) and is considered an important archive for past rainfall information stored in the layers of its wood (Robertson et al., 2006; Slotta et al., 2017; Woodborne et al., 2015, 2016, 2018). Facing the potential impacts of climate change, *A. digitata* can, on the one hand, help in understanding past climate patterns in order to better model future climate scenarios across the African continent, a great challenge considering the current lack of high-resolution trans-regional proxy data (IPCC, 2007, 2013). On the other hand, baobabs may be threatened by recent climate warming as the mortality of monumental baobabs in southern Africa has increased over the last decade (Patrut et al., 2018), although the species probably has endured more severe climate conditions during earth history. In this respect, conclusive evidence is lacking and a better understanding is required of the ecophysiology of baobabs, their response to varying temperature and rainfall in general, and to extremes like drought but also heavy rainfall events as from cyclones that can occur in parts of their distribution area (e.g. South Africa, Mozambique or Oman).

Stable isotopes ($\delta^{13}C$, $\delta^{18}O$) incorporated in the cellulose extracted from wood and, where applicable, also tree-ring width were shown to correlate significantly with climate parameters (Robertson et al., 2006; Woodborne et al., 2015, 2016; Slotta et al., 2017). However, dendroclimatological approaches are hampered by the baobab's complex wood anatomy. A baobab tree ring generally consists of a diffuse porous wood section dominated by fibers and vessels followed by a terminal parenchyma band (TPB). Since the stems are specialized for water storage, parenchyma cells make up 69-88 % of their total wood content (Chapotin et al., 2006a). Apart from TPBs, parenchyma cells occur paratracheal vasicentric, forming a sheath around associated vessels, as well as apotracheal (not associated with vessels and irregularly dispersed among fibers) in fine bands or clusters or even as rays (Fisher, 1981; Neumann et al., 2001; Rajput, 2004; Wickens and Lowe, 2008). The high abundance of parenchymal tissue can cause difficulties in distinguishing TPBs from other tangentially orientated non-annual parenchyma bands throughout the wood, especially because the thickness of TPBs can vary greatly around the stem (Chapotin et al., 2006c; Slotta et al., 2017). Ring counting on baobabs of known age can result in about 98 % accuracy of the actual tree age (Guy, 1970), but even opposing radii of the same individual may differ in absolute numbers (Johansson, 1999). UV light induced fluorescence was found to be very helpful in identifying the wood anatomical details of baobab trees (Slotta et al., 2017). Nevertheless, false and missing rings together with differences in tree age and site of origin caused conventional cross-dating to fail (Slotta et al., 2017).

https://doi.org/10.5194/bg-2019-325
Preprint. Discussion started: 26 August 2019
© Author(s) 2019. CC BY 4.0 License.

Selection criteria of dendroecological or -climatological study sites usually include locations close to the ecological limit of a species to ensure a clearer signal of the limiting environmental and climatic factors (Fritts, 1976; Smith, 2008). Baobabs growing in the Dhofar region of Oman occupy the north-eastern range of the species' natural distribution (Wickens and Lowe, 2008). The woodlands and forests along the Dhofar mountains are a paleo-African relict of a moist vegetation belt that once stretched beyond the Southern Arabian Peninsula into Asia (Kürschner et al., 2004; Hildebrandt and Eltahir, 2006). Upwelling at the southern coast of Oman lowers the Arabian Sea's surface temperature and consequently the moist air masses of the southwest monsoon winds. Once the dew point is reached, fog and low clouds form and then drift inshore against the mountain range (Kürschner et al., 2004). Compared to other distributions of baobabs, this site is therefore characterized by mostly horizontal precipitation (i.e. collection of cloud water within the canopy; Hildebrandt and Eltahir, 2006). Nevertheless, the climate is defined by a single wet season and should thus favor the formation of tree rings.

Where tree rings are anatomically non-distinct, intra-annual analysis of stable isotopes ($\delta^{13}C$, $\delta^{18}O$) can help to identify annual growth patterns (e.g. Poussart et al., 2004; Anchukaitis et al., 2008; Pons and Helle, 2011; Xu et al., 2014; Ohashi et al., 2016). The high sensitivity of stable isotopes to external drivers, such as weather conditions, and internal drivers, such as species-specific physiology, makes them a valuable tool to reconstruct the environmental influences during tree growth (e.g. Fichtler et al., 2010; Hartl-Meier et al., 2015; Szejner et al., 2016; van der Sleen et al., 2017). Elevated $\delta^{13}C$ values in tree-rings are mainly caused by a reduction in stomatal conductance (as a result of drought stress) and/or an increase in photosynthetic activity (Scheidegger et al., 2000). In both cases the leaf internal CO_2 concentration declines and leads to a reduced enzymatic discrimination against ^{13}C (Farquhar et al., 1982; Farquhar and Cernusak, 2012). However, since increased photosynthetic activity is unlikely under drought stress, high $\delta^{13}C$ values are typically interpreted as a drought signal in areas where growth is limited by moisture availability (Brienen et al., 2011; Schollaen et al., 2013; Woodborne et al., 2015, 2016). Following this approach, the higher the $\delta^{13}C$ values become, the more severe the drought episode. $\delta^{18}O$ in tree rings reflect soil water $\delta^{18}O$, originating from precipitation and modified by plant physiological influences, including leaf-water ^{18}O enrichment due to evapotranspiration and biological fractionation during metabolic processes (Roden et al., 2000; Kahmen et al., 2011; Treydte et al., 2014 and citations therein). $\delta^{18}O$ in tree rings from (sub-)tropical timber has been proven to strongly represent the isotopic composition of rain, i.e. the source-water (e.g. Evans and Schrag, 2004; Brienen et al., 2012, 2013; Boysen et al., 2014; Baker et al., 2015; Baker et al., 2016; van der Sleen et al., 2015, 2017). Variation of $\delta^{18}O$ in rainfall is determined by several factors where the amount of rain (Araguas et al., 1996) plays a key role producing a strong inverse correlation.

Reliable age estimates of tropical and subtropical trees can be obtained from radiocarbon dating (Swart, 1963; Worbes, 1989). Using the bomb peak caused by extensive nuclear testing in the 1950s and 60s, radiocarbon dating was proven a reliable tool in plant sciences that enables dendrochronological studies on trees with indistinct growth boundaries (Fichtler et al., 2003; Hua et al., 2003; Robertson et al., 2006; Andreu-Hayles et al., 2015; Ohashi et al., 2016; Baker et al., 2017; Linares et al., 2017). The vast majority of bomb tests have been carried out in the Northern Hemisphere. A delay in atmospheric mixing resulted in five different zones (three in the Northern Hemisphere, two in the Southern Hemisphere)

https://doi.org/10.5194/bg-2019-325
Preprint. Discussion started: 26 August 2019
© Author(s) 2019. CC BY 4.0 License.

which were separated by atmospheric cell boundaries (Fig. 1A) (Hua et al., 2013). Despite an increasing number of studies that reconstruct the atmospheric radiocarbon content of the bomb peak period from tree rings (e.g. Hua et al., 2013; Turney et al., 2018), tree-ring radiocarbon studies to particularly refine zones close to the equator (NH3, SH3) are still lacking.

We performed highly resolved inter- and intra-annual radiocarbon and stable isotope measurements on tree-ring cellulose of a baobab tree from Oman in order to (1) fill the existing gap for atmospheric ^{14}C data ($F^{14}C$) between the African continent and India, and (2) to produce a securly dated annual time series of baobab wood increment growth and stable isotope ratios ($\delta^{13}C$, $\delta^{18}O$). The accurate time series of tree-ring width index (RWI), minimum ($\delta^{13}C_{min}$, $\delta^{18}O_{min}$), maximum ($\delta^{13}C_{max}$, $\delta^{18}O_{max}$) and mean ($\delta^{13}C_{mean}$, $\delta^{18}O_{mean}$) stable isotope values where then (3) compared to instrumental climate data for assessing their sensitivity to moisture related quantities including a comparison of intra-ring stable isotope courses to drought, as well as to pre- and post-monsoonal heavy rainfall events from cyclones.

2 Materials and Methods

2.1 Study site and climate

The baobab tree analyzed for this study is one of more than 60 individuals growing in Wadi Hinna (17°03' N, 54° 36' E, 318 meters above sea level (m asl)) at the edge of the Dhofar Mountains in southern Oman (Fig. 1B, D). The Dhofar Mountains reach elevations of about 1,450 m asl and are separated from the Arabian Sea by a narrow coastal plain. The prevailing wind system is defined by four different seasons (Walters and Sjoberg, 1990; Charabi et al., 2011): (1) winter (December-March), in which the region is dominated by the Northeast Monsoon, (2) the spring transition (April-May), during which the NE circulation breaks down while south-westerly trade winds enter the region; (3) summer (mid June-mid September), in which damp air masses of the Southwest Monsoon (also *khareef*) encounter the mountain range and bring dense fog and light rain (Kwarteng et al., 2009) and (4) the autumn transition (October-November), during which the north-easterly flow is re-established.

The closest meteorological station is located at Salalah airport (17° 01' N, 54° 04' E, 20 m asl), 57 km west from Wadi Hinna. Due to the distance and altitudinal difference between station and study site, the use of interpolated grid data seemed more reasonable. The mean annual temperature is 23.1 °C (1945-2013; CRU TS4.01, modified after Harris et al. 2013). Precipitation data from the Climate Research Unit (CRU TS4.01, modified after Harris et al. 2013) and the Global Precipitation Climatology Centre (GPCC V7_05, (Schneider et al., 2015)) covering the study site (17.0-17.5° N, 54.0-54.5° S) was tested for statistical similarity against data from the Salalah station (1945-2013) in order to check which data set is best representing the temporal variability of the study region. Hereby, GPCC data showed the highest correlation ($r_{GPCC} = 0.91$, $p < 0.0001$; $r_{CRU} = 0.70$, $p < 0.0001$) and was therefore chosen for further analysis. The grid cell suggests an average annual precipitation of 130 mm that varies strongly interannually (range: 28-534 mm; 1945-2013). The light drizzle during *khareef* accounts for about 70 % (= 90 mm, range: 21-231 mm) of the average annual rainfall. Apart from the monsoon rain, precipitation is rare and erratic, originating either from low pressure systems moving across Oman or from

https://doi.org/10.5194/bg-2019-325
Preprint. Discussion started: 26 August 2019
© Author(s) 2019. CC BY 4.0 License.

cyclonic systems moving westward from the Arabian Sea during the spring (May-June) and autumn (October-November) transitions (Clark et al., 1987). These tropical storms with heavy rainfall occur about once every three years (Pedgley, 1969; Hildebrandt and Eltahir, 2006; Strauch et al., 2014). Aside from intensity and duration, rainfall from the monsoon and cyclones usually differs distinctively in its respective isotopic signature (Clark et al., 1987; Strauch et al., 2014; Wushiki, 1991) (Fig. 1C, Table 1). Monsoon precipitation from the Dhofar mountains generally correlates with the oxygen isotopic composition of the Indian monsoon rainfall along the southeast coast of Oman (Strauch et al., 2014) and varies little between -0.5 ‰ and +0.7 ‰. The values are close to the mean $\delta^{18}O$ of 0.61 ± 0.02 ‰ reported for the Arabian Sea water (Lambs et al., 2011). Virtually no difference exists in the oxygen isotopic signature of monsoon rain, fog and interception waters (Table 1). In contrast, water samples collected in the Dhofar mountains from cyclones with sometimes one or more years' worth of rainfall amount in a single day show highly variable but significantly negative $\delta^{18}O$ signatures down to -11 ‰, depending on isotope fractionation due to the amount effect (Dansgaard, 1964).

2.2 Field work

The sampling took place in early April 2015 when the trees were still without leaves. Ten baobabs were sampled in total. Increment cores of 12 mm in diameter and up to 80 cm in length were taken at breast height from four different orientations (NE, SE, SW, and NW). The samples were stored airtight and cool and after fieldwork kept in a freezer to prevent mold formation and distortion of wood anatomical features due to drying.

2.3. Sample preparation and wood increment dissection

The baobab tree showed rather wide growth rings favorable for intra-annual analyses, possibly due its immediate proximity to an ephemeral stream. The SW oriented core was chosen because its parenchyma bands were very distinct and the perpendicular cut vessels and fibers allowed for precise subsampling. The core surface was prepared with a razor blade perpendicular to the longitudinal stem growth and photographs were taken with a fluorescence microscope (Nikon MULTIZOOM AZ100M, V-2A: 380-420 nm; camera head: Nikon digital sight DS-Fi1c; light source: C-HGFI HG Precenteres Fiber Illumiator (130 W mercury lamp); program: NIS Elements 4.30.01© 1991-2014 Laboratory Imaging). The stitched panorama of the core pictures was printed for further sampling documentation (scale 1:7.6) and provided the basis for the tree-ring width measurements (Fig. 2).

For the intended radiocarbon and stable isotope analyses, tangential wood slices of approximately 1 mm were cut parallel to the fiber orientation, in radial direction from the cambial zone towards the pith. The entire bomb peak and the decade before was dissected amounting to a total of 360 samples representing resolutions from just 1 up to 11 samples per year.

Visible rays and other identified parenchymatous structures were removed from the wood slices to avoid possible contamination, because parenchyma cells can undergo cell division within the stem, independent from the vascular cambium (Chapotin et al., 2006a; Spicer, 2014). Hence, we were aware that cellulose from parenchyma may therefore carry a different radiocarbon and stable carbon isotope signal than the surrounding wood vessels and fibers. A potential fraction of

https://doi.org/10.5194/bg-2019-325
Preprint. Discussion started: 26 August 2019
© Author(s) 2019. CC BY 4.0 License.

parenchyma cells in between vessels and fibers was originally considered being small of higher order. Two thirds of each wood slice were separated for radiocarbon dating while the remaining third was kept for stable isotope analyses. Terminal parenchyma bands (TPBs) were kept as a whole and used for radiocarbon analysis, only.

2.4 Radiocarbon dating

110 samples were holocellulose extracted with a base-acid-base-acid-bleaching procedure after (Němec et al., 2010). Ten samples were further purified to alpha-cellulose with an additional base treatment (17.5 % NaOH for 2 h at room temperature) followed by washing and freeze-drying. The cellulose samples were then graphitized using an Automated Graphitization Equipment (AGE III) coupled to an elemental analyzer (EA: Vario MICRO cube; Wacker et al., 2010b). Once graphitized, the samples were immediately pressed into targets to minimize their interaction with air and their ^{14}C content was measured with a MICADAS mass spectrometer (Wacker et al., 2010a). Since the tree ring structure for the outermost wood section is often hard to interpret (Johansson, 1999; Slotta et al., 2017), we did a five-point screening for the bomb peak before samples were selected from each of the clearly-identifiable growth rings onwards from what we thought to be 1942. We abstained from sampling older tree rings because of a lack of reliable precipitation data beyond this date. With intention to minimize possible carry-over effects from the implementation of previous years' non-structural carbohydrates (NSC) into the current year's wood cellulose, the samples for dating were selected from the last third of each growth structure while steering clear of the TPB by at least one sample, where possible (Fig. 2). For comparison, five individual TPBs were analyzed for 1960-1963 (n = 4) and 2005. For the period between 2005 and 2015, for which by visual inspection annual rings could not be identified, 19 samples were dissected of which 17 samples were dated. In addition, intra-ring radiocarbon analysis was performed on the tree rings of 1962 (6 samples) and 1963 (8 samples).

Comparison of ^{14}C of the assumed tree rings with atmospheric ^{14}C data comprising the bomb peak values (see different zones in Fig. 1A) allowed for annual dating between 1956 and 1980; before and after, differences between the atmospheric ^{14}C values of consecutive years differed not sufficiently enough for secure annual designation of wood increments (see Hua et al., 2003). The normalized ^{14}C activity ratio ($F^{14}C$) of the assumed tree rings was plotted against and correlated peak-to-peak (± 5 years) with the calibration curve for the corresponding hemispheric zone NH3 (Hua et al., 2013). Because of an observed offset in the data sets, the calibration curves for SH3 and SH1-2 (Hua et al., 2013) were also included in the comparison (Fig. 3). The baobab samples' position on the time axis is relative to their position within the tree ring of a growing season lasting from June until September. In case of suspected missing rings, the wood anatomy was reviewed and additional samples were dated. No properly dated tree-ring width chronology (e.g. from juniper) from the study region is currently available for comparison. To rule out possible missing rings before 1956 and after 1980, we visually and statistically cross-dated the baobab time series with the seasonally and annually resolved precipitation amount (May-Sep, Jun-Sep, and Jan-Dec) for the grid cell 17-17.5° N, 54-54.5° E (GPCC V7.05, Schneider et al. 2015). Calendar ages were calculated from the $F^{14}C$ values of the TPBs using the program OxCal v4.3.2 (Bronk Ramsey, 2017) and the post-bomb atmospheric NH3 and SH1-2 curves (Hua et al., 2013).

https://doi.org/10.5194/bg-2019-325
Preprint. Discussion started: 26 August 2019
© Author(s) 2019. CC BY 4.0 License.

Biogeosciences Discussions Open Access EGU

2.5 Stable isotope analysis

For the stable isotope analyses ($\delta^{13}C$, $\delta^{18}O$), all 360 samples (excluding TPBs) were holocellulose extracted after Wieloch et al. (2011), homogenized by ultrasonic treatment (Laumer et al., 2009), and freeze-dried for at least 48 h before 130-180 µg of cellulose and reference material, respectively, were packed in silver capsules and stored over night at 100 °C in a vacuum drying oven. Simultaneous dual measurements of $\delta^{13}C$ and $\delta^{18}O$ were performed on carbon monoxide derived from high temperature TC/EA pyrolysis (1400 °C) coupled online via a Conflo IV to an IRMS Delta V Plus (Thermo Fisher Scientific, Bremen, Germany). Values are referred to VPDB and VSMOW, respectively with a reproducibility of ≤ 0.15 for $\delta^{13}C$ and ≤ 0.25 for $\delta^{18}O$.

In order to use $\delta^{13}C$ of baobab tree-ring cellulose ($\delta^{13}C_{raw}$) as a measure for plant response to weather conditions, the $\delta^{13}C_{raw}$ values have been corrected ($\delta^{13}C^*$) for the anthropogenic changes in the long term trend of the atmospheric CO_2 source. Rising atmospheric CO_2 concentrations (pCO_2) and correspondingly declining $\delta^{13}C$ of atmospheric CO_2 ($\delta^{13}CO_2$) prevailing since the onset of industrialization (1850 AD) were addressed by subtracting for each tree-ring stable isotope value the annual changes in $\delta^{13}CO_2$, obtained from direct measurements (White et al., 2015). Since trees respond to increased atmospheric pCO_2 with higher discrimination against ^{13}C an additional moderate correction of 0.073‰ per 10 ppm change (Kürschner, 1996) was applied producing a corrected $\delta^{13}C^*$ record.

The intra-annual isotopic signatures were plotted against their relative position within the tree ring normalized to 100 % of the respective tree-ring width. Annual tree-ring stable isotope values were obtained from averaging intra-ring $\delta^{13}C^*$ and $\delta^{18}O$ values.

2.6 Statistical analysis

Ring widths were measured for the entire core and detrended using an exponential fit (R program, package dplR; Bunn et al., 2018) resulting in a ring-width index chronology (RWI). Due to different intra-annual resolution of the stable isotope time series, ranging from 2 to 11 samples per year, the actual intra-annual signature might be blurred and thus may weakening the sensitivity of intra-ring isotopic records. Hence, we particularly tested minimum ($\delta^{13}C^*_{min}$, $\delta^{18}O_{min}$) and maximum ($\delta^{13}C^*_{max}$, $\delta^{18}O_{max}$) stable isotope values for their climate sensitivity, besides mean isotopic signatures ($\delta^{13}C^*_{mean}$, $\delta^{18}O_{mean}$).

The obtained time series (RWI, $\delta^{13}C^*_{min/max/mean}$, $\delta^{18}O_{min/max/mean}$) were tested for autocorrelation. Moving mean, variance and correlation tests (window size = 15 years) were performed to discretize the timeseries in terms of central tendency, variation and trend behavior. The response of these parameters to weather conditions was then evaluated by calculating the Pearson correlation with monthly and seasonally averaged data of precipitation (GPCC V7.05, Schneider et al. 2015), cloud cover, temperature ($T_{min/max/mean}$), and vapor pressure (CRU TS4.01) for the grid cell 17-17.5° N, 54-54.5° E, as well as relative humidity anomaly (CRU_blendnewjul08_RH_7303cf) for the cell 15-20° N, 20-25° E. The impact of drought on the wood parameters was estimated using the standardized precipitation evapotranspiration index (SPEI) for the grid cell 17-17.5° N, 54-54.5° E. SPEI assesses droughts by using both precipitation and temperature variability at different

https://doi.org/10.5194/bg-2019-325
Preprint. Discussion started: 26 August 2019
© Author(s) 2019. CC BY 4.0 License.

timescales (Vicente-Serrano et al., 2010a; 2010b; 2015). Where applicable, the coefficient of determination (COD = $r^2 \cdot 100$ %) has been added for explanatory meaning.

3 Results

3.1 Wood anatomy

The TPBs were generally well defined in this ca. 100-year old tree, with a mean width of 1.5 mm (range: 0.5-2.4 mm). The only exceptions were the outermost 15.3 mm of wood and three rings with TPB widths ≤ 0.1 mm (i.e. 1973, 1981, 1982) which were finally confirmed by the radiocarbon dating. In general, the width of the TPBs was significantly correlated to the width of the corresponding tree ring ($r_0 = 0.45$, $COD_0 = 20.3$ %, $p < 0.001$), as well as the rings that were built 1 to 4 years earlier (highest correlation: $r_{-4} = 0.36$, $COD_{-4} = 13.0$ %, $p = 0.005$) and those built 1-2, as well as 6 years later (highest correlation: $r_{+1} = 0.47$, $COD_{+1} = 22.0$ %, $p < 0.001$).

The mean tree-ring width for the analyzed period (TRW measured without TPBs and excluding missing rings) was 4.8 ± 2.2 mm with a slightly significant negative trend over time (r = -0.32, COD = 10.2 %, $p = 0.011$). After detrending, significant autocorrelations were observed for lags 1-3 and lag 6. The moving mean test revealed major changes in the central tendency of the RWI time series for the periods 1962-1965, 1976-1977, and 1985-1992. No major changes were revealed in the variance homogeneity and linear dependency.

3.1 Radiocarbon measurements and dating

3.1.1 Holocellulose vs. alpha cellulose

Six out of ten pairs of holocellulose and alpha cellulose values are equal within two standard deviations and nine out of ten within three standard deviations. Hence, we refrained from performing the additional extraction step.

3.1.2 Inter-annual $F^{14}C$ variabiltity

The baobab $F^{14}C$ values of the assumed tree rings (excluding the outer wood part without clearly identifiable TPBs) fit the overall shape of the bomb peak curve, thus proving their annual character (Fig. 3). Disproportional data leaps led to a review of the wood anatomy and consequently the identification of three more tree rings (boundaries marked by dashed lines in Fig. 2) while the year 1975 is regarded as absent from our time series. This interpretation of the $F^{14}C$ data was confirmed by visual and statistical comparison of the TRW chronology with precipitation data. The comparison with precipitation data also approved missing rings for the years 1951 and 1983, as year-to-year variability of atmospheric $F^{14}C$ data was not sufficient for unambiguous detection. The last identifiable TPB corresponds to the tree ring of 2005, thus, the outermost 15.3 mm of wood represented nine years of growth (2006-2014) that could not be distinguished. Due to the shallow slope of

https://doi.org/10.5194/bg-2019-325
Preprint. Discussion started: 26 August 2019
© Author(s) 2019. CC BY 4.0 License.

the calibration curve during this period, we abstained from assigning the measured $F^{14}C$ values to a specific year. Hence, the final annually dated baobab time series investigated further covers the period from 1941 till 2005.

The highest correlation between the revised baobab time series and calibration curves from different hemispheric zones (Fig. 3A, B) was reached for a peak-to-peak fit with SH1-2, although the study site is located in zone NH3 (Fig. 1A) ($r = 0.996$, $p < 0.0001$; SH3: $r = 0.995$, $p < 0.0001$; NH3: $r = 0.989$, $p < 0.0001$, all CODs > 97.8 %). For the peak period (1964-1966) baobab $F^{14}C$ values were found notably lower than the mean values of the zone NH3 (≈ -8.8 %) and even slightly lower than the mean values of SH1-2 (≈ -2.6 %) (Fig. 3A, B).

3.1.3 Intra-annual $F^{14}C$ variability

Intra-annual baobab $F^{14}C$ values analyzed for the two consecutive years 1962 and 1963 were found positioned between the higher NH3 and the lower SH1-2 atmospheric values (Fig. 3B). The $F^{14}C$ values for the TPBs ($F^{14}C_{TPB}$) for 1960-1962 ($n = 3$) are significantly higher than the (mean) values for the corresponding tree rings (Fig. 3, Table 2) and also higher than expected for NH3. For 1963, the $F^{14}C_{TPB}$ value is in the range of the tree ring's value, and the last clearly visible TPB (2005) shows a slightly lower $F^{14}C$ value than the corresponding tree ring. Based on radiocarbon TPBs appear to be younger on average than the fibers and vessels of their corresponding tree ring (Table 2).

3.2 Statistical characteristics of tree-ring parameter time series

Despite the corrections made for atmospheric change in $\delta^{13}C$ and pCO_2, the $\delta^{13}C^*$ time series shows a slightly negative trend over time ($r = -0.32$, COD = 10.2 %, $p = 0.011$) (Fig. 4). The mean $\delta^{13}C^*$ value was -26.99 ± 1.21 ‰ (min: -29.77 ‰, max: -23.43 ‰) with an observed mean range per year of 2.27 ‰ (maximum range: 4.55 ‰ in 1963). $\delta^{13}C^*_{max}$ correlated with RWI ($r = 0.31$, COD = 9.6 %, $p = 0.014$) and strongly with $\delta^{18}O_{max}$ ($r = 0.61$, COD = 37.2 %, $p < 0.0001$). Significant autocorrelations were found for $\delta^{13}C^*_{max}$ (lag 3) and considerably declining for $\delta^{13}C^*_{mean}$ (lag 1-2 and $\delta^{13}C^*_{min}$ (lag 1). The moving tests revealed major changes in the central tendency of $\delta^{13}C^*_{min}$ for the periods 1948-1953, 1960-1961, and 1984-1985. Major changes in the linear dependency of $\delta^{13}C^*_{max}$ occurred in 1964-1966 and 1984-1985 and its variance homogeneity changed significantly for 1985-1987.

The mean $\delta^{18}O$ value was 30.44 ± 0.77 ‰ (min: 27.77 ‰, max: 32.67 ‰) with an observed mean range per year of 1.38 ‰ (maximum range: 3.16 ‰ in 2002). A strong correlation was found between $\delta^{18}O_{min}$ and RWI ($r = -0.60$, $p < 0.0001$). No significant autocorrelation was found for any of the $\delta^{18}O$ time series. Major changes in the central tendency occurred for $\delta^{18}O_{min}$ in 1984-1987 and for $\delta^{18}O_{max}$ in 1968-1969. The variance homogeneity of $\delta^{18}O_{min}$ changed significantly for 1957-1959, 1976-1977, 1985-1988, and 1991-1993; the variance homogeneity of $\delta^{18}O_{max}$ significantly for 1959-1961.

3.3 Intra-annual stable isotope courses

The intra-annual signature was found similar for both $\delta^{13}C^*$ and $\delta^{18}O$ (all years with > 1 value; $n = 59$; Fig. 5A). The first half of the tree ring was characterized by a majority of minimum values per year, whereas the second half comprised mainly

https://doi.org/10.5194/bg-2019-325
Preprint. Discussion started: 26 August 2019
© Author(s) 2019. CC BY 4.0 License.

maximum values. This separation was clearer for $\delta^{13}C^*$ where 86 % of all $\delta^{13}C^*_{min}$ occurred within the first half (64 % within the first quarter) and 80 % of all $\delta^{13}C^*_{max}$ were found in the second half of the tree ring (58 % within the last quarter). $\delta^{18}O$ showed a generally higher variability, with the minimum and maximum values more scattered throughout the year. Only 68 % of the $\delta^{18}O_{min}$ were found within the first half of a tree ring (44 % within the first quarter) and 71 % of the $\delta^{18}O_{max}$ occurred within the second half (44 % within the last quarter). The mid-section showed the highest variation for both $\delta^{13}C^*$ and $\delta^{18}O$, the values at the very beginning and the very end varied less. Due to different resolutions of the intra-annual time series ranging from 2 to 11 samples per year, the actual intra-annual isotope courses might be blurred. The time series with a minimum of 7 samples per year (n = 20) resulted in a more distinct intra-ring course (Fig. 5B). For $\delta^{18}O$, the values were still more scattered than for $\delta^{13}C^*$ with only 75 % of $\delta^{18}O_{min}$ occurring in the first half (35 % within the first quarter) and 85 % of $\delta^{18}O_{max}$ occurring in the second half of the tree ring (55 % within the last quarter). The center of the tree ring revealed a short-term dip in $\delta^{18}O$ before rising towards the end of the tree ring, which is in contrast to $\delta^{13}C^*$ that showed slightly lowered, but not declining values in the mid-section (Fig. 5B).

3.3.1 Intra-annual isotope course in years with heavy rainfall events due to spring or autumn cyclones

In order to estimate the influence of heavy rainfall events on the intra-annual $\delta^{13}C^*$ and $\delta^{18}O$, we separated years with pre- to early and late to post-monsoonal storms (starting in Apr/May/Jun or Sep/Oct/Nov, respectively) ≥ 90 mm (i.e. average monsoon precipitation) from other years with > 1 or ≥ 7 (Fig. 5A, B) observations, respectively. As shown in Fig. 5C this revealed a pronounced difference in the mid-section of the intra-ring isotope courses, causing a significant decline. In years with spring cyclones (n = 5; 1959, 1963, 1977, 1989, 2002), the $\delta^{13}C^*$ and $\delta^{18}O$ values declined during the first half of a tree ring and steeply increased within the second half, reaching their maximum close to or at the end of each tree ring. Although $\delta^{13}C^*$ and $\delta^{18}O$ courses resemble very much, $\delta^{18}O$ showed a more pronounced decline in the mid-section and a higher spread of values, with maximum values in two out of five years at the very beginning of a tree ring (Fig. 5C). Hence, minimum values are shifted from the beginning of an intra-ring isotope course to its center in years with spring cyclones and rainfall ≥ 90 mm.

The very few years with autumn cyclones (Fig. 6A; n = 2) indicated a final decrease in $\delta^{13}C^*$ (after reaching the maximum values) at the end of a tree ring, but no distinct pattern. $\delta^{18}O$ responds largely similar to autumn cyclones with the lowest values of the intra-ring course in the last quarter of the tree ring. Additionally, $\delta^{18}O$ values were found above normalized average in the first half of the intra-ring $\delta^{18}O$ course, and below average at the end (Fig. 6A, right). The tree ring of 1948 showed a conspicuously strong increase in $\delta^{18}O$ towards the very end. It was rather wide and is represented by 8 intra-annual isotope samples.

https://doi.org/10.5194/bg-2019-325
Preprint. Discussion started: 26 August 2019
© Author(s) 2019. CC BY 4.0 License.

Biogeosciences Discussions Open Access EGU

3.3.2 Intra-annual isotope course in years with exceptionally low monsoon precipitation

Years with less than 50 % of the average monsoon precipitation (Jun-Sep: ≤ 45 mm) and no spring/autumn heavy rainfall due to cyclones were selected for inspecting the influence of drought on the intra-ring stable isotope courses. Six years with reduced average monsoon precipitation were identified (1968, 1972, 1974, 2000, 2001, 2003). Except for the year 2000, all intra-ring $\delta^{13}C^*$ courses start with a distinct increase reaching $\delta^{13}C^*_{max}$ or values close to $\delta^{13}C^*_{max}$ within the first half of the tree ring (Fig. 6B). In 1968, 1972 and 2003 $\delta^{13}C^*$ kept increasing at lower rates to a $\delta^{13}C^*_{max}$ towards the end of each ring, while declining in 1974, 2000 and 2001 within the second half of the tree ring. In 1974 $\delta^{13}C^*$ was reaching lower values at the end than at the beginning of the tree ring. $\delta^{18}O$ was found mainly rising to a maximum within the first half of the tree ring and then declining towards the end. Only 2003 showed a continuous rise of $\delta^{18}O$ with decreasing incline towards the maximum value at the end of the tree ring. The intra-annual course for the year 2000 showed a much higher intra-ring stable isotope variation, but it was also the year with the most observations (= 6) for a year with low monsoon rain. In sum, both isotope species generally showed rather similar intra-ring trends in response to drought with high to highest values in the mid-section of the intra-ring course (Fig. 6B).

3.4 Statistical relations between weather conditions and tree-ring parameters

Significant correlations of RWI, $\delta^{13}C^*_{min/mean/max}$, and $\delta^{18}O_{min/mean/max}$ with climate quantities indicative for the moisture conditions at the site were observed for the current and the previous year (Table 3, Fig. 7). RWI, comprising total annual increment growth, showed significant positive correlations ($p < 0.001$) with August and May-September precipitation (Table 3, Fig. 7A). $\delta^{13}C^*_{mean}$ generally revealed no relation to precipitation amount and only weak correlations with other climate data. In contrast, $\delta^{18}O_{mean}$ correlated significantly negative with precipitation of May and other periods (May-Sep, Jan-Dec).

Intra-ring minimum isotope values displayed only weak correlations between $\delta^{13}C^*_{min}$ and precipitation of previous year January and current year November and no relations to other climate quantities. Conversely, $\delta^{18}O_{min}$ correlated significantly with T_{max} and all moisture related climate quantities, with strongest relationship to precipitation of pre-monsoonal May (Table 3, Fig. 7B).

$\delta^{13}C^*_{max}$ showed more and better relationships with climate quantities than $\delta^{13}C^*_{mean}$ and $\delta^{13}C^*_{min}$. Significant correlations were found for May temperature, vapor pressure, and SPEI (1 month). The highest correlation to cloud cover was revealed for $\delta^{18}O_{max}$ in pre-monsoon April (Table 3, Fig. 7C). Further significant correlations of $\delta^{18}O_{max}$ were also found with the climate conditions of the previous year (previous Jan-Dec, Feb, Oct and Nov; c.f. Table 3 for details).

https://doi.org/10.5194/bg-2019-325
Preprint. Discussion started: 26 August 2019
© Author(s) 2019. CC BY 4.0 License.

Biogeosciences Discussions

4 Discussion

4.1 $F^{14}C$ values in baobab wood are very likely altered by carbohydrate metabolism

Situated in Oman, the baobab $F^{14}C$ values were expected to fit the post-bomb atmospheric curve NH3 (Hua et al., 2013). However, they were found notably lower than NH3 and even SH3, around the bomb peak period (1964-1967, Fig. 3A). A potential influencing factor to be addressed might be the close proximity to the coast of the Arabian Sea, where upwelling of nutrient and carbon rich waters causes an outgassing of 'older' CO_2 into the atmosphere (Takahashi et al., 2009; Sreeush et al., 2018) that dilutes the bomb peak signal. But this dilution effect should also be seen in pre-bomb peak $F^{14}C$ data. Since the measurements for the 1940s are consistent with other records for the northern hemisphere, we rule out a significant influence of the upwelling. The baobab record of the bomb peak is further characterized as a period of major changes in the central tendency of RWI (1962-1965) as well as in the linear dependency of $\delta^{13}C^*_{max}$ (1964-1966). It is difficult to assess the driving force(s) behind these major changes, however, the notably lowered values of baobab $F^{14}C$ during the bomb peak period may to some extend be explained by the baobabs' carbohydrate turnover. The observed autocorrelation in the $\delta^{13}C^*$ signature points to the use of previous years' carbon for part of the growth, which leads to a dampening in the carbon isotope record of environmental signals, including the atmospheric $F^{14}C$ content. The dramatic deviation of baobab $F^{14}C$ values and atmospheric NH3 data around the bomb peak area points out that an immediate allocation of leaf assimilates to wood growth is very unlikely and transient storage or carbon recycling from respiration has to be considered.

In an attempt to explain the observed baobab $F^{14}C$ values, we applied a simple conceptual modeling approach assuming that baobab wood formation is fueled by pools of non-structural carbon (NSC) that carry the atmospheric $F^{14}C$ source values for the NH3 zone. From radiocarbon dating Richardson et al. (2013) found a mean age of stemwood NSC of about 10 years in temperate forest trees with individual dates of up to 31 years. They presented lines of evidence for 'fast' and 'slow' cycling reserves and proposed a two-pool model structure to explain the age of stemwood total NSC. A follow-up study on the mixing of new and previously stored NSC supported this model and the 'last in, first out' hypothesis (Richardson et al., 2015). We have no ^{14}C data or other information about the age of different NSC pools in baobabs, however, we attempted to address these considerations by assuming two NSC pools and tested for annual renewal rates ranging between 2 and 10% ('slow' cycling reserves) and 98 to 90% (low contribution of old reserves; 'fast' cycling), respectively. Taking the 'last in, first out' hypothesis (Richardson et al., 2015) into account we further presumed that wood formation is fueled by a mix from these two NSC pools and visually tested the agreement with the observed baobab $F^{14}C$ values for relative contributions between 95% and 70% from the `fast`cycling pool and 5 to 30% from the `slow`cycling NSC pool. Best approximation to the baobab $F^{14}C$ time series was achieved by holding stakes of 85% `fast`cycling and 15% 'slow' cycling NSCs with annual renewal rates of 95% (renewal `fast`cycling pool) and 5% (renewal `slow`cycling pool) of the two respective pools (Fig. 8). The `slow`cycling NSC pool may predominantly represent starch the major long-term carbohydrate reserve in trees, although starch has not always been found older than sugars which should represent the `fast`cycling NSC pool (Richardson et al. 2015). We suggest that the `slow`cycling NSC might as well originate from considerable cortical photosynthesis (Kotina et

https://doi.org/10.5194/bg-2019-325
Preprint. Discussion started: 26 August 2019
© Author(s) 2019. CC BY 4.0 License.

Biogeosciences Discussions

al., 2017) of older respiratory CO_2. Additionally, the significant autocorrelation found for $\delta^{13}C^*$ strongly indicates the incorporation of previous years' carbon into tree-ring cellulose from either carbohydrate reserves and/or from current carbohydrates derived from old stem respiratory CO_2 recycled in cortical photosynthesis.

Despite our simplistic approach with assumptions based on literature data from very different tree species and not taking into account pool size dynamics, the offset in $F^{14}C$ between baobab cellulose and NH3 data during the time around the bomb peak is well captured. Nonetheless, baobab $F^{14}C$ for 1945, 1952-1954, 1956 and 1957 lie slightly above the calculated range of $F^{14}C$ of the NSC pool. Although to a much lesser extent, this is in common with $F^{14}C$ values measured for the TPBs indicating that the wood of these rings may have contained an unrecognized high fraction of intraxylary parenchyma cells and did not consist of pure xylem fibres and vessels.

4.2 $F^{14}C$ of TPBs indicates ongoing formation and/or restructuring of parenchyma tissue for several years

Terminal parenchyma bands (TPBs), marking the visual tree-ring boundaries, were found to be at least up to 1.6 years younger than the corresponding tree ring when calibrated with post bomb NH3 and assigned to the youngest possible age (Table 2, Fig. 8). In addition, the highest correlation between the width of TPBs and RWI was found for the ring built one year after the corresponding tree ring. Initial parenchyma bands are being produced each year initiated by the cambium between wood (xylem) and bark. However, well-defined TPBs could only be found deeper in the xylem, marking well the actual tree-ring boundaries, but also explaining previously described difficulties in cross-dating the outer part of baobab core samples (Johansson, 1999; Slotta et al., 2017).

Since parenchyma cells retain their ability to divide throughout their lifespan (Spicer, 2014) it is thus possible that the proliferation, i.e. post-cambial parenchyma growth, starts once the existing storage volume is sufficiently refilled. This point in time may vary, depending on the tree's current water and nutrient budget, and may sometimes not be reached at all. However, parenchyma tissue may carry a generally different radiocarbon signal than the surrounding wood vessels and fibers, although both types of xylem are likely being fed by the same mixed NSC pool with the only difference being that fibers and vessels are annual and parenchyma cells are perennial and can undergo structural changes for an unknown number of years. Fractions of parenchyma tissue in between vessels and fibers might be easily overlooked during the sample dissection procedure causing a potential shift in $F^{14}C$ towards younger ages. The assumed lifespan is based on the significant correlation found between the width of TPBs and the width of rings built 6 years later. However, the TPBs seem to be more variable in their ^{14}C content than vessels and fibers. Probably, because their growth is not continuous, but rather discontinuous during their life following the year of initialization. Presumably, parenchyma growth depends on NSC availability and the demand of water, as well as the supply of water by the soil. A significant post-cambial growth, i.e. widening of TPBs could not be observed for 1973, 1981, and 1982, which is two years before the missing tree ring in 1975 and one and two years before the missing tree ring in 1983. This leads to the assumption that baobabs prioritize growth of fibres and vessels over storage enlargement, i.e. formation of new parenchyma cells. When there is not enough energy to invest in growth, baobabs seem to refrain from broadening the initial TPBs. However, the ten TPBs prior to the missing ring

https://doi.org/10.5194/bg-2019-325
Preprint. Discussion started: 26 August 2019
© Author(s) 2019. CC BY 4.0 License.

410 in 1951 were all notably thickened; the reason for this missing ring remains unclear. The fact that TPBs accounting for nine years (2006-2014) were not well-developed in the outer part of the wood core potentially indicates a particularly high stress level over the last decade, which is in line with the meteorological data, i.e. increasing T_{max} and decreasing precipitation (Fig. 4).

In sum, the relatively high fraction (69-88 %) (Chapotin et al., 2006c) and perennial character of parenchyma tissue in 415 stem succulent baobabs lead to shifts of the atmospheric $F^{14}C$ signal in their wood. The relative content and lifetime of intraxylary parenchyma may be also considered when reconstructing atmospheric $F^{14}C$ from tree rings of other woody plant groups. Conifers were found to have the lowest parenchyma fractions, followed by angiosperm trees (including shrubs), woody climbers (lianas) and succulents (Morris et al., 2016). Major differences in the relative parenchyma content of angiosperms were also found between tropical species (36.2 ± 13.4 %) and temperate species (21.1 ± 7.9 %) (Morris et al., 420 2015), i.e. the atmospheric $F^{14}C$ signal in tree-ring cellulose may be altered in a species specific and/or even plant individual way. This, however, does only play a role in radiocarbon dating exercises utilizing the bomb peak with its dramatic changes over a few years.

4.3 Baobabs have annual growth rings, but visual recognition depends on tree-ring width and shaping of the TPBs

425 Besides the issues discussed above, the high number of radiocarbon dates allowed to confirm the annual nature of the baobab growth zones. Very thin TPBs (≤ 0.1 mm) cannot not be identified as such with a solely wood anatomical approach. From this study, only xylem increments of ≥ 2 mm in combination with TPBs of ≥ 0.5 mm thickness can be considered an annual tree ring with confidence. Thus, a high number of radiocarbon dates is advisable to date time series of centuries-old baobab wood samples for climate reconstruction purposes not only because of varying external growth conditions, but also because 430 baobabs show varying growth rates during the different phases within their stem development (Breitenbach, 1985) and because very old individuals are often multi-stemmed (e.g. Patrut et al., 2015b). However, annual time resolution appears to be possible particularly for wood sections with ample ring width and distinct TPBs. Here, we worked with fresh samples, stored airtight and cool to not distort the original wood anatomical characteristics. When air-drying baobab, the wood shrinks and, in some cases reveals fissures between the TPBs and the part of a tree ring that is dominated by fibers and vessels. 435 Assuming those fissures to mark actual tree-ring boundaries, individual growth rings for stable isotope and/or radiocarbon sampling have been peeled off for paleoclimatic studies (e.g. Woodborne et al. 2015, 2016). This sampling strategy waives the elaborate securing of freshly taken increment cores (c.f. Sampling strategy) on the expense of not obtaining exact growth increment data. Another constraint is that formation of more than one parenchyma band per year can easily introduce substantial uncertainty in tree-ring counting. In this study, 3 missing rings were detected in a time series of 65 years from a 440 rather well-grown young individual suggesting that errors of 5 % or more have to be considered. It has also to be noted, that the sampling procedure based on dry wood will hardly allow to deduce intra-ring isotope signals, as from this study design.

https://doi.org/10.5194/bg-2019-325
Preprint. Discussion started: 26 August 2019
© Author(s) 2019. CC BY 4.0 License.

Biogeosciences Discussions Open Access EGU

Nonetheless, precipitation reconstructions of good quality from $\delta^{18}O$ of baobab tree-ring cellulose seem to be possible, as $\delta^{18}O_{mean}$ revealed highly significant correlations with the May-September period (Table 3).

4.4 Intra-annual stable isotope courses are in line with isotope fractionation theory

The intra-annual stable isotope courses were rather similar for both $\delta^{13}C^*$ and $\delta^{18}O$ (Fig. 5). The first half of the tree ring was characterized by a majority of minimum values per year, whereas the second half comprised mainly maximum values. In terms of intra-annual $\delta^{13}C^*$ the observed seasonal course is very different to the recurring pattern described for deciduous tree species from temperate (Helle and Schleser, 2004) and tropical zones (Schollaen et al., 2013), where maximum $\delta^{13}C$ values were generally observed during early wood formation indicative for the use of ^{13}C enriched reserves like starch at the beginning of the vegetation period. Conversely, the baobab's seasonal $\delta^{13}C$ pattern generally showed low to lowest values at the beginning of each tree ring which points to the use of other, ^{13}C-depleted, non-structural carbohydrates that might be stemming from cortical photosynthesis (Kotina et al., 2017) producing assimilates with 'lighter' $\delta^{13}C$ compared to those from leaf photosynthesis (Cernusak et al., 2001). Additionally, the significant autocorrelation found for $\delta^{13}C^*$ strongly indicates the incorporation of previous years' carbon into tree-ring cellulose from either carbohydrate reserves and/or from current carbohydrates derived from old stem respiratory CO_2 recycled in cortical photosynthesis. Unlike for $\delta^{13}C^*$, no autocorrelation was present in $\delta^{18}O$. A lack of significant autocorrelation in $\delta^{18}O$ series from tree-ring cellulose is quite common (Treydte et al., 2007), however, this could not be expected here per se considering the relatively large water saving capacity of baobab stem wood potentially storing varying amounts of mixed precipitation waters from several monsoon seasons. Baobabs draw upon their water reserves when flushing leaves prior to the onset of the monsoon season (Chapotin et al., 2006b) which may lead to a very high annual turnover diminishing potential autocorrelation in $\delta^{18}O$ of stem, i.e. source water. Despite the differences in autocorrelation, $\delta^{18}O$ intra-ring values revealed a higher variability than those of $\delta^{13}C^*$. This may point to the fact that the source water (precipitation) isotopic signature already does contain a climatic signal related to air temperature and precipitation amount, whereas $\delta^{13}C$ of atmospheric CO_2 does not. Highly variable rainfall amounts from pre- or post-monsoonal cyclones comprise correspondingly variable $\delta^{18}O$ signatures (Fig. 1C). Climate relevance of tree ring $\delta^{13}C$ is originating only from fractionation processes during photosynthetic CO_2 uptake. Nonetheless, the overall high similarity between the average intra-annual $\delta^{13}C^*$ and $\delta^{18}O$ courses suggests that stable isotope fractionations at leaf level (Farquhar et al., 1989; Roden et al., 2000; Kahmen et al., 2011), where water and carbon cycles meet during photosynthesis, are of predominant importance. In accordance with fractionation theories, maximum values at or close to the end of the tree ring likely do correspond to the end of the monsoon period, when relative humidity is getting low and leaf-to-air vapor pressure deficit is rising, thus causing corresponding leaf water ^{18}O enrichment to increase while enzymatic discrimination against ^{13}C during photosynthetic uptake of atmospheric CO_2 is declining.

https://doi.org/10.5194/bg-2019-325
Preprint. Discussion started: 26 August 2019
© Author(s) 2019. CC BY 4.0 License.

4.5 Intra-annual stable isotope courses are indicative for years with heavy rainfall events from cyclones

Starting with low to intermediate values intra-ring $\delta^{13}C^*$ and $\delta^{18}O$ of the mid-section either increase or decline in dry or wet years, respectively. In particular, heavy pre-monsoonal rainfall from spring cyclones did not significantly alter start and end values but apparently causes a distinct decline in the mid-section of the general stable isotope course (Fig. 5C). In general, pre-monsoonal precipitation can help to replenish the stem water content during and/or shortly after leaf flush and its influence on the baobabs' ecophysiology is also been reflected by the significant correlations of $\delta^{18}O_{min}$ in Apr-May and with RWI in May (Table 3, Fig. 7A, B). However, strongly depleted $\delta^{18}O$ signatures of heavy pre-monsoonal rainfall events are not imprinted into the intra-ring $\delta^{18}O$ pattern as a deep, short-term dip, but rather lead to a distinct trough in the mid-section. This points to a lagging, or more indirect influence by diluting the $\delta^{18}O$ signature of the stem water and/or by causing wetter (micro-)site conditions evoking reduced leaf water ^{18}O enrichment, but also increased ^{13}C discrimination at the beginning and during main monsoon season. Note, isotopically lighter values for the mid-section were observed also with increasing number of observations per year. $\delta^{18}O$ courses from wide tree rings with more than 7 observations per year revealed a short-term mid-section decline (Fig. 5B, right) resulting from higher monsoon precipitation as suggested by the significant correlations with RWI (Table 3). The expression of this dip within the intra-annual $\delta^{18}O$ pattern is relatively weak, however, it may hamper the clear detection of unknown spring cyclonic events in potential future reconstruction studies.

Only two years (1948, 2004) with autumn cyclones bringing more than 90 mm of rain could be investigated (Fig. 6A) Due to the lack of replication, a conclusive evaluation of intra-ring stable isotope response to post-monsoonal cyclones is not possible, especially with respect to the observed indistinct $\delta^{13}C^*$ courses (Fig. 6A, left). However, $\delta^{18}O$ seems to largely respond to autumn cyclones with a strong decline to very low values in the last quarter of the intra-ring course. When compared to the average seasonal $\delta^{18}O$ course and those for years with spring cyclones, intra-ring $\delta^{18}O$ values of years with autumn cyclones were found above in the first half, and below at the end of the tree-ring (Fig. 6A, right). Furthermore, post-monsoonal rain seems to prolong the growing season as indicated by the rather wide tree ring of 1948 that provided 8 intra-annual isotope samples. The conspicuously strong increase in $\delta^{18}O$ towards the very end might reflect evaporative ^{18}O enrichment of the soil water uptaken by the tree and/or effects due to increased evapotranspiration at leaf level during the prolonged growing period after a heavy autumn rainfall event. In sum, the intra-ring stable isotope courses are modified by pre- and post-monsoonal rainfall events from cyclones. Significantly negative correlations of $\delta^{18}O_{max}$ with cloud cover for previous October and the current April also indicate an influence of non-monsoonal precipitation (Table 3, Fig. 7C). Hence, baobabs might well take advantage of rainfall outside their actual vegetation period.

4.6 Increased stable isotope values in mid-section of intra-annual courses reflect low monsoon precipitation

A clearer picture with more constrained intra-ring isotope patterns was obtained for dry years with less than 50 % of the average monsoon precipitation and no pre- or post-monsoonal cyclones. Except for the year 2000 all $\delta^{13}C^*$ and $\delta^{18}O$ courses reveal increased values for the mid-section of a tree ring (Fig. 6B). The very low variability of $\delta^{18}O$ in rain or fog within and

https://doi.org/10.5194/bg-2019-325
Preprint. Discussion started: 26 August 2019
© Author(s) 2019. CC BY 4.0 License.

between different monsoon seasons (Table 1) suggests that the observed $\delta^{18}O$ pattern has to be largely attributed to the effects of fractionation processes at leaf level. Vapor pressure deficit between leaves and ambient air is higher during a dry monsoon season causing enhanced ^{18}O enrichment in leaf water and lower stomatal conductance with decreased leaf internal CO_2 concentrations causing photosynthetic ^{13}C discrimination to decline. Decreasing values at the very end of an annual stable isotope course can be observed in $\delta^{13}C^*$ of three years (1974, 2000, 2001) and in $\delta^{18}O$ of all but one year (2003), which might be attributed to the decreasing transpiration and reduced photosynthesis towards the end of the growing period, i.e. during leaf senescence. $\delta^{13}C^*$ of 1968, 1972 and 2003 did not reach the high values of the other dry years' tree rings, however, in the second half they continue to increase (at a slower rate) to the end. This trend may or may not be an artefact of the low resolution (3 values per year) causing a more or less linear increasing trend (c.f. Fig. 6A). The year 2000 showed an unexpected early decline in $\delta^{18}O$, as seen for spring storm years, that might be due to the previous year's October precipitation. Unfortunately, this finding cannot be verified for other years because the tree rings following other fall storms were only half as wide and the signal is probably lost in the resolution.

5 Conclusions

This study comprises 62 years of highly resolved inter- and intra-annual analyses of $F^{14}C$, $\delta^{13}C$ and $\delta^{18}O$ on baobab tree-ring cellulose. The fairly high number of radiocarbon dates has confirmed that baobabs have annual growth rings that are separated by terminal parenchyma bands. However, unambiguous visual recognition of tree-rings was possible only for xylem increments of ≥ 2 mm in combination with TPBs of ≥ 0.5 mm thickness. Situated in Oman, the baobab $F^{14}C$ values were expected to fit the post-bomb atmospheric curve NH3. However, they were found notably lower than NH3 and even lower than SH3 around the bomb peak period (1964-1967). Normally, three radiocarbon samples placed within the bomb peak period result in a very precise dating. But, with the bomb peak represented by clearly lower $F^{14}C$ values compared to the corresponding atmospheric zone, a lower sampling rate on the baobab would have likely led to a misinterpretation of the time series' resolution and duration. A conceptual modeling approach suggests that the observed shift between atmospheric and baobab $F^{14}C$ is caused by a mixture of non-structural carbohydrates fueling baobab wood formation with 85% contribution from a `fast`cycling and 15% from a 'slow' cycling pool with respective annual renewal rates of 95% (renewal `fast`cycling pool) and 5% (renewal `slow`cycling pool). Radiocarbon dates of terminal parenchyma bands, marking the visual tree-ring boundaries, were found to be at least up to 1.6 years younger than their corresponding tree ring. This can be explained by the well-known ongoing restructuring and/or formation of new intraxylary parenchyma tissue years after initial tree-ring formation. Stem succulent baobabs have a very high fraction of long-lived parenchyma tissue that is not only arranged in tangential bands but also irregularly dispersed within the wood modifying its $F^{14}C$ values. Hence, the relative content and lifetime of intraxylary parenchyma may be also considered when reconstructing atmospheric $F^{14}C$ from tree rings of other woody plant groups or when dating particularly parenchyma-rich succulent plants. Nonetheless, the high-resolution bomb-peak dating approach together with visual inspection of TPBs allows the development of precise time series

https://doi.org/10.5194/bg-2019-325
Preprint. Discussion started: 26 August 2019
© Author(s) 2019. CC BY 4.0 License.

useful for investigating the ecophysiology of baobabs to assess their vulnerability to the recent climate change. Well dated longer time series for paleoclimatic reconstructions are still more difficult to establish, although annual time resolution appears to be possible for wood sections with ample ring width and distinct TPBs. Tree-ring width indices (RWI) and stable isotope ratios have revealed significant climate sensitivity. RWI and intra-ring $\delta^{18}O_{min}$ correlated well with each other ($r = -0.6$, $p < 0.0001$) and with precipitation amount for the period from pre-monsoon May to the end of the monsoon season in September-October. Intra-annual stable isotope courses were found rather similar for both $\delta^{13}C$ and $\delta^{18}O$. The distinct pattern seems indicative for years with heavy rainfall events from pre-monsoonal cyclones. Rain from post-monsoonal cyclones may also be recorded, however, a conclusive evaluation was not possible because of only two years of observation. Years with particularly low monsoon rain were reflected by increased stable isotope values in mid-section of intra-annual courses. When intra-ring isotope signals, as from this study, cannot be deduced, precipitation reconstructions of good quality from cellulose $\delta^{18}O$ seem to be possible, as $\delta^{18}O_{mean}$ revealed highly significant correlations with the May-September period. Overall, in the baobab archive $\delta^{18}O$ appeared to be a good climate proxy followed by tree-ring width and $\delta^{13}C$.

Acknowledgements

We are grateful to the Director General of Nature Conservation Suleiman Bin Nasser Al Akhzami and the Director of Biodiversity D. Thuraya Said Al-Sariri at the Ministry of Environment & Climate affairs for granting us permission (Permit No. 11/2015) to sample baobab trees in Wadi Hinna and to the Ministry employees involved in the collection process for their field assistance. Furthermore, we would like to extend our gratitude to Bernhard Pracejus and Frank Mattern (Sultan Qaboos University) for collaboration. Frank Mattern and his wife Sarah as well as Annette Kossler and Heidemarie Pettauer also assisted in the field. We are also grateful to Quan Hua for making available published radiocarbon data. We would further like to thank Silvia Bollhalder, and Philip Gautschi (ETH Zurich) for their support in the laboratory and Andreas Hendrich for his help with the figure layout. We acknowledge the fruitful discussions with Arne Ramisch and thank Patrick Lynch for the linguistic revision of the manuscript. This study was funded by the DFG (HE3089/10-1, RI 809/32-1) and supported with ^{14}C measurements performed at the Laboratory of Ion Beam Physics (Prof. H.A. Synal) at ETH Zurich.

Data availability

The data produced in this publication will be available from the PANGAEA database.

Supplement

There is supplement related to this article.

© Author(s) 2019. CC BY 4.0 License.

Author contributions

FS, FR, GH and LW conceived the study. Field work for this study was conducted by FS and FR. FS and LW performed the $F^{14}C$ analyses. FS and GH performed chemical extraction of tree-ring cellulose and measurements of stable isotope ratios of carbon and oxygen. FS and GH prepared the manuscript with contributions from all co-authors.

Competing interests

The authors declare that they have no conflict of interest.

References

Anchukaitis, K. J., Evans, M. N., Wheelwright, N. T., and Schrag, D. P.: Stable isotope chronology and climate signal calibration in neotropical montane cloud forest trees Journal of Geophysical Research: Biogeosciences 113, 1-17, doi:10.1029/2007JG000613, 2008.

Andreu-Hayles, L., Santos, G. M., Herrera-Ramirez, D. A., Martin-Fernandez, J., Ruiz-Carrascal, D., Boza-Espinoza, T. E., Fuentes, A. F., and Jorgensen, P. M.: Matching denrochronological dates with the southern hemisphere C-14 bomb curve to confirm annual tree rings in *Pseudolmedia rigida* from Bolivia, Radiocarbon, 57, 1-13, doi:10.2458/azu_rc.57.18192, 2015.

Araguas, L. A., Danesi, P., Froehlich, K., and Rozanski, K.: Global monitoring of the isotopic composition of precipitation, J Radioan Nucl Ch Ar, 205, 189-200, 1996.

Baker, J. C. A., Hunt, S. F. P., Clerici, S. J., Newton, R. J., Bottrell, S. H., Leng, M. J., Heaton, T. H. E., Helle, G., Argollo, J., Gloor, M., and Brienen, R. J. W.: Oxygen isotopes in tree rings show good coherence between species and sites in Bolivia, Global and Planetary Change, 133, 298-308, doi:10.1016/j.gloplacha.2015.09.008, 2015.

Baker, J. C. A., Gloor, M., Spracklen, D. V., Arnold, S. R., Tindall, J. C., Clerici, S. J., Leng, M. J., and Brienen, R. J. W.: What drives interannual variation in tree ring oxygen isotopes in the Amazon?, Geophysical Research Letters, 43, 11831-11840, doi:10.1002/2016gl071507, 2016.

Baker, J. C. A., Santos, G. M., Gloor, M., and Brienen, R. J. W.: Does *Cedrela* always form annual rings? Testing ring periodicity across South America using radiocarbon dating, Trees-Structure and Function, 31, 1999-2009, doi:10.1007/s00468-017-1604-9, 2017.

Becker, J. J., Sandwell, D. T. , Smith, W. H. F., Braud, J., Binder, B., Depner, J., Fabre, D., Factor, J., Ingalls, S.,Kim, S-H., Ladner, R., Marks, K., Nelson, S., Pharaoh, A., Sharman, G., Trimmer, R., Von Rosenburg, J., Wallace, G., Weatherall., P.: Global Bathymetry and Elevation Data at 30 Arc Seconds Resolution: SRTM30_PLUS, Marine Geodesy, 32:4, 355-371, 2009.

Boysen, B. M. M., Evans, M. N., and Baker, P. J.: delta O-18 in the Tropical Conifer *Agathis robusta* Records ENSO-Related Precipitation Variations, Plos One, 9, 9, doi:10.1371/journal.pone.0102336, 2014.

© Author(s) 2019. CC BY 4.0 License.

Breitenbach, F. v.: Aantekening oor die groeitempo van aangeplante kremetartbome (*Adansonia digitata*) en opmerkinge ten opsigte van lewenstyd, groeifases en genetiese variasie van die spesie, Dendrologiese Tydskrif, 5, 1-21, 1985.

Brienen, R. J. W., Wanek, W., and Hietz, P.: Stable carbon isotopes in tree rings indicate improved water use efficiency and drought responses of a tropical dry forest tree species, Trees, 25, 103-113, doi:10.1007/s00468-010-0474-1, 2011.

Brienen, R. J. W., Helle, G., Pons, T. L., Guyot, J.-L., and Gloor, M.: Oxygen isotopes in tree rings are a good proxy for Amazon precipitation and El Nino-Southern Oscillation variability, Proceedings of the National Academy of Sciences of the United States of America, 109, 16957-16962, doi:10.1073/pnas.1205977109, 2012.

Brienen, R. J. W., Hietz, P., Wanek, W., and Gloor, M.: Oxygen isotopes in tree rings record variation in precipitation delta O-18 and amount effects in the south of Mexico, Journal of Geophysical Research-Biogeosciences, 118, 1604-1615, doi:10.1002/2013jg002304, 2013.

Bronk Ramsey, C.: Methods for summarizing radiocarbon datasets, Radiocarbon, 59, 1809-1833, 2017.

Bunn, A., Korpela, M., Biondi, F., Campole, F., Mérian, P., Qeadan, F., Zang, C., Pucha-Cofrep, D., and Wernicke, J.: dplR: Dendrochronology Program Library in R, 2018.

Cernusak, L. A., Marshall, J. D., Comstock, J. P., and Balster, N. J.: Carbon isotope discrimination in photosynthetic bark, Oecologia, 128, 24-35, doi:10.1007/s004420100629, 2001.

Chapotin, S. M., Razanameharizaka, J. H., and Holbrook, N. M.: Water relations of baobab trees (*Adansonia* spp. L.) during the rainy season: does stem water buffer daily water deficits?, Plant Cell and Environment, 29, 1021-1032, doi:10.1111/j.1365-3040.2005.01456.x, 2006a.

Chapotin, S. M., Razanameharizaka, J. H., and Holbrook, N. M.: Baobab trees (*Adansonia*) in Madagascar use stored water to flush new leaves but not to support stomatal opening before the rainy season, New Phytologist, 169, 549-559, doi:10.1111/j.1469-8137.2005.01618.x, 2006b.

Chapotin, S. M., Razanameharizaka, J. H., and Holbrook, N. M.: Abiomechanical perspective on the role of large stem volume and high water content in baobab trees (*Adansonia spp.*; Bombacaceae), American Journal of Botany, 93, 1251-1264, doi:10.3732/ajb.93.9.1251, 2006c.

Charabi, Y., Al-Yahyai, S., and Gastli, A.: Evaluation of NWP performance for wind energy resource assessment in Oman. , Renewable and Sustainable Energy Reviews 15, 1545-1555, 2011

Clark, I., Fritz, P., Quinn, O., Rippon, P., Nash, H., and Al-Said, S.: Modern and fossil groundwater in an arid environment: a look at the hydrogeology of southern Oman, Proc. Symp. on Isotope Techniques in Water Resources Development. IAEA (Int. At. Energy Agency), Vienna, 1987, 167-187,

Dansgaard, W.: Stable isotopes in precipitation, Tellus, 16, 437-468, 1964.

Evans, M. N., and Schrag, D. P.: A stable isotope-based approach to tropical dendroclimatology, Geochimica et Cosmochimica Acta, 68, 3295-3305, 2004.

https://doi.org/10.5194/bg-2019-325
Preprint. Discussion started: 26 August 2019
© Author(s) 2019. CC BY 4.0 License.

Farquhar, G. D., O'Leary, M. H., and Berry, J. A.: On the Relationship between Carbon Isotope Discrimination and the Intercellular Carbon Dioxide Concentration in Leaves, Australian Journal of Plant Physiology, 9, 121-137, doi:10.1071/PP9820121 1982.

Farquhar, G. D., Ehleringer, J. R., and Hubick, K. T.: Carbon isotope discrimination and photosynthesis, Annu. Rev. Plant Physiol. Plant Mol. Biol., 40, 503-537, 1989.

Farquhar, G. D., and Cernusak, L. A.: Ternary effects on the gas exchange of isotopologues of carbon dioxide, Plant, Cell & Environment, 35, 1221-1231, doi:10.1111/j.1365-3040.2012.02484.x, 2012.

Fichtler, E., Clark, D. A., and Worbes, M.: Age and Long-term Growth of Trees in an Old-growth Tropical Rain Forest: Based on Analyses of Tree Rings and ^{14}C, Biotropica, 35, 306-317, 2003.

Fichtler, E., Helle, G., and Worbes, M.: Stable-carbon isotope time series from tropical tree rings indicate a precipitation signal, Tree-Ring Research, 66, 35-49, 2010.

Fisher, J. B.: Wound healing by exposed secondary xylem in *Adansonia* (Bombacaceae), IAWA Bulletin n.s., 2, 193-199, doi:10.1163/22941932-90000732, 1981.

Fritts, H. C.: Tree Rings and Climate, Academic Press Inc., London, UK, 1976.

Hartl-Meier, C., Zang, C., Büntgen, U., Esper, J., Rothe, A., Gottlein, A., Dirnbock, T., and Treydte, K.: Uniform climate sensitivity in tree-ring stable isotopes across species and sites in a mid-latitude temperate forest, Tree Physiology, 35, 4-15, doi:10.1093/treephys/tpu096, 2015.

Helle, G., and Schleser, G. H.: Beyond CO_2-fixation by Rubisco - an interpretation of C-13/C-12 variations in tree rings from novel intra-seasonal studies on broad-leaf trees, Plant Cell and Environment, 27, 367-380, 2004.

Hildebrandt, A., and Eltahir, E. A. B.: Forest on the edge: Seasonal cloud forest in Oman creates its own ecological niche, Geophysical Research Letters, 33, doi:10.1029/2006GL026022, 2006.

Hua, Q., Barbetti, M., Zoppi, U., Chapman, D. M., and Thomson, B.: Bomb Radiocarbon in Tree Rings from Northern New South Wales, Australia: Implications for Dendrochronology, Atmospheric Transport, and Air-Sea Exchange of CO_2, Radiocarbon, 45, 431-447, doi:10.1017/S0033822200032793, 2003.

Hua, Q., Barbetti, M., and Rakowski, A. Z.: Atmospheric Radiocarbon for the Period 1950–2010, Radiocarbon, 55, 2059-2072, doi:10.2458/azu_js_rc.v55i2.16177, 2013.

IPCC: Climate Change 2007: Impacts, Adaptions and Vulnerability. Contribution of working group II to the Fourth Assessment Report of the Intergovernmental Panel on Climate Change, Cambridge, UK, 2007.

IPCC: Climate Change 2013: The Physical Science Basis. Contribution of Working Group I to the Fifth Assessment Report of the Intergovernmental Panel on Climate Change, Cambridge, UK, New York, NY, USA, 2013.

Johansson, M.: The Baobab tree in Kondoa Irangi Hills, Tanzania, Minor Field Studies, 74, 1999.

Kahmen, A., Sachse, D., Arndt, S. K., Tu, K. P., Farrington, H., Vitousek, P. M., and Dawson, T. E.: Cellulose $\delta^{18}O$ is an index of leaf-to-air vapor pressure difference (VPD) in tropical plants, PNAS, 108, 1981-1986, doi:10.1073/pnas.1018906108, 2011.

© Author(s) 2019. CC BY 4.0 License.

665 Kotina, E. L., Oskolski, A. A., Tilney, P. M., and Van Wyk, B. E.: Bark anatomy of *Adansonia digitata* L. (Malvaceae), Adansonia, 39, 31-40, doi:10.5252/a2017n1a3, 2017.

Kürschner, H., Hein, P., Kilian, N., and Hubaishan, M. A.: The Hybantho durae-*Anogeissetum dhofaricae* ass. nova-phytosociology, structure and ecology of an endemic South Arabian forest community, Phytocoenologia, 34, 569-612, 2004.

Kürschner, W. M.: Leaf stomata as biosensors of palaeoatmospheric CO_2 levels., LPP Contributions Series, 5, 1-152, 1996

670 Kwarteng, A. Y., Dorvlo, A. S., and Vijaya Kumar, G. T.: Analysis of a 27-year rainfall data (1977–2003) in the Sultanate of Oman, International Journal of Climatology, 29, 605-617, doi:10.1002/joc.1727, 2009.

Lambs, L., Gurumurthy, G. P., and Balakrishna, K.: Tracing the sources of water using stable isotopes: first results along the Mangalore-Udupi region, south-west coast of India, Rapid Communications in Mass Spectrometry, 25, 2769-2776, doi:10.1002/rcm.5104, 2011.

675 Laumer, W., Andreu, L., Helle, G., Schleser, G. H., Wieloch, T., and Wissel, H.: A novel approach for the homogenization of cellulose to use micro-amounts for stable isotope analyses, Rapid Communications in Mass Spectrometry, 23, 1934-1940, doi:10.1002/Rcm.4105, 2009.

Linares, R., Santos, H. C., Brandes, A. F. N., Barros, C. F., Lisi, C. S., Balieiro, F. C., and de Faria, S. M.: Exploring the C-14 bomb peak with tree rings of tropical species from the Amazon rain forest, Radiocarbon, 59, 303-313,

680 doi:10.1017/rdc.2017.10, 2017.

Morris, H., Plavcova, L., Cvecko, P., Fichtler, E., Gillingham, M., Martinez Cabrera, H., McGlinn, D., Wheeler, E., Zheng, J., Ziemińska, K., and Jansen, S.: A global analysis of parenchyma tissue fractions in secondary xylem of seed plants, New Phytologist, 209, 1553-1565, doi:10.1111/nph.13737, 2016.

Němec, M., Wacker, L., Hajdas, I., and Gäggeler, H.: Alternative methods for cellulose preparation for AMS measurement,

685 Radiocarbon, 52, 1358-1370, doi:10.1017/S0033822200046440, 2010.

Neumann, K., Schoch, W., Détienne, P., and Schweingruber, F. H.: Woods of the Sahara and Sahel: an anatomical atlas / Bois du Sahara et du Sahel: atlas d'anatomie / Hölzer der Sahara und des Sahel: ein anatomischer Atlas, edited by: Birmensdorf, E. F. W., Haupt Verlag, Bern, 2001.

Ohashi, S., Durgante, F. M., Kagawa, A., Kajimoto, T., Trumbore, S. E., Xu, X. M., Ishizuka, M., and Higuchi, N.: Seasonal

690 variations in the stable oxygen isotope ratio of wood cellulose reveal annual rings of trees in a Central Amazon terra firme forest, Oecologia, 180, 685-696, doi:10.1007/s00442-015-3509-x, 2016.

Patrut, A., Woodborne, S., Patrut, R. T., Hall, G., Rakosy, L., Von Reden, K. F., Lowy, D., and Margineanu, D.: Radiocarbon dating of African baobabs with two false cavities: The investigation of Luna tree, Stud. Univ. Babes-Bolyai Chem., 60, 7-20, 2015a.

695 Patrut, A., Woodborne, S., von Reden, K. F., Hall, G., Hofmeyr, M., Lowy, D. A., and Patrut, R. T.: African Baobabs with False Inner Cavities: The Radiocarbon Investigation of the Lebombo Eco Trail Baobab, Plos One, 10, 13, doi:10.1371/journal.pone.0117193, 2015b.

© Author(s) 2019. CC BY 4.0 License.

Patrut, A., Woodborne, S., Patrut, R. T., Rakosy, L., Hall, G., Ratiu, I.-A., and Von Reden, K. F.: Final Radiocarbon Investigation of Platland Tree, the Biggest African Baobab, Studia Universitatis Babeș-Bolyai Chemia, 62, 347-354, doi:10.24193/subbchem.2017.2.27, 2017.

Patrut, A., Woodborne, S., Patrut, R. T., Rakosy, L., Lowy, D. A., Hall, G., and von Reden, K. F.: The demise of the largest and oldest African baobabs, Nature Plants, 4, 423-426, doi:10.1038/s41477-018-0170-5, 2018.

Pedgley, D. E.: Cyclones along the Arabian coast, Weather, 24, 456-470, 1969.

Pons, T. L., and Helle, G.: Identification of anatomically non-distinct annual rings in tropical trees using stable isotopes, Trees-Structure and Function, 25, 83-93, doi:10.1007/s00468-010-0527-5, 2011.

Poussart, P. F., Evans, M. N., and Schrag, D. P.: Resolving seasonality in tropical trees: multi-decade, high-resolution oxygen and carbon isotope records from Indonesia and Thailand, Earth and Planetary Science Letters, 218, 301-316, 2004.

Rajput, K. S.: Formation of Unusual Tissue Complex in the Stem of *Adansonia digitata* Linn. (Bombacaceae), Beiträge zur Biologie der Pflanzen, 73, 331-342, 2004.

Richardson, A. D., Carbone, M. S., Keenan, T. F., Czimczik, C. I., Hollinger, D. Y., Murakami, P., Schaberg, P. G., and Xu, X.: Seasonal dynamics and age of stemwood nonstructural carbohydrates in temperate forest trees, New Phytologist, 197, 850-861, doi:10.1111/nph.12042, 2013.

Richardson, A. D., Carbone, M. S., Huggett, B. A., Furze, M. E., Czimczik, C. I., Walker, J. C., Xu, X., Schaberg, P. G., and Murakami, P.: Distribution and mixing of old and new nonstructural carbon in two temperate trees, New Phytologist, 206, 590-597, 2015.

Riedel, F., Henderson, A. C. G., Heussner, K. U., Kaufmann, G., Kossler, A., Leipe, C., Shemang, E., and Taft, L.: Dynamics of a Kalahari long-lived mega-lake system: hydromorphological and limnological changes in the Makgadikgadi Basin (Botswana) during the terminal 50 ka, Hydrobiologia, 739, 25-53, doi:10.1007/s10750-013-1647-x, 2014.

Robertson, I., Loader, N. J., Froyd, C. A., Zambatis, N., Whyte, I., and Woodborne, S.: The potential of the baobab (*Adansonia digitata* L.) as a proxy climate archive, Applied Geochemistry, 21, 1674-1680, doi:10.1016/j.apgeochem.2006.07.005, 2006.

Roden, J. S., Lin, G. G., and Ehleringer, J. R.: A mechanistic model for interpretation of hydrogen and oxygen isotope ratios in tree-ring cellulose, Geochimica et Cosmochimica Acta, 64, 21-35, 2000.

Scheidegger, Y., Saurer, M., Bahn, M., and Siegwolf, R.: Linking stable oxygen and carbon isotopes with stomatal conductance and photosynthetic capacity: a conceptual model, Oecologia, 125, 350-357, doi:10.1007/s004420000466, 2000.

Schneider, U., Becker, A., Finger, P., Meyer-Christoffer, A., Rudolf, B., and Ziese, M.: GPCC Full Data Reanalysis Version 7.0 at 0.5°: Monthly Land-Surface Precipitation from Rain-Gauges built on GTS-based and Historic Data. , Ed 7.0, Global Precipitation Climatology Centre (GPCC, http://gpcc.dwd.de/) at Deutscher Wetterdienst 2015.

Schollaen, K., Heinrich, I., Neuwirth, B., Krusic, P. J., D'Arrigo, R. D., Karyanto, O., and Helle, G.: Multiple tree-ring chronologies (ring width, delta C-13 and delta O-18) reveal dry and rainy season signals of rainfall in Indonesia, Quaternary Science Reviews, 73, 170-181, doi:10.1016/j.quascirev.2013.05.018, 2013.

© Author(s) 2019. CC BY 4.0 License.

Slotta, F., Helle, G., Heussner, K. U., Shemang, E., and Riedel, F.: Baobabs on Kubu Island, Botswana - A dendrochronological multi-parameter study using ring width and stable isotopes ($\delta^{13}C$, $\delta^{18}O$), Erdkunde, 71, 23-43, doi:10.3112/erdkunde.2017.01.02, 2017.

Smith, K. T.: An organismal view of dendrochronology, Dendrochronologia, 26, 185-193, doi:10.1016/j.dendro.2008.06.002, 2008.

Spicer, R.: Symplasmic networks in secondary vascular tissues: parenchyma distribution and activity supporting long-distance transport, J Exp Bot, 65, 1829-1848, doi:10.1093/jxb/ert459, 2014.

Sreeush, M. G., Valsala, V., Pentakota, S., Prasad, K. V. S. R., and Murtugudde, R.: Biological production in the Indian Ocean upwelling zones–Part 1: refined estimation via the use of a variable compensation depth in ocean carbon models, Biogeosciences, 115, 1895-1918, doi:10.5194/bg-15-1895-2018, 2018.

Strauch, G., Al-Mashaikhi, K. S., Bawain, A., Knoller, K., Friesen, J., and Muller, T.: Stable H and O isotope variations reveal sources of recharge in Dhofar, Sultanate of Oman, Isotopes in Environmental and Health Studies, 50, 475-490, doi:10.1080/10256016.2014.961451, 2014.

Swart, E. R.: Age of the Baobab Tree, Nature, 198, 708-709, doi:10.1038/198708b0, 1963.

Szejner, P., Wright, W. E., Babst, F., Belmecheri, S., Trouet, V., Leavitt, S. W., Ehleringer, J. R., and Monson, R. K.: latitudinal gradients in tree-ring stable carbon and oxygen isotopes reveal differential climate influences of the North American Monsoon System., J. Geophys. Res. Biogeosciences 121, 1978-1991, doi:10.1002/2016JG003460, 2016.

Takahashi, T., Sutherland, S. C., Wanninkhof, R., Sweeney, C., Feely, R. A., Chipman, D. W., Hales, B., Friederich, G., Chavez, F., Sabine, C., Watson, A., Bakker, D. C. E., Schuster, U., Metzl, N., Yoshikawa-Inoue, H., Ishii, M., Midorikawa, T., Nojiri, Y., Körtzinger, A., Steinhoff, T., Hoppema, M., Olafsson, J., Arnarson, T. S., Tilbrook, B., Johannessen, T., Olsen, A., Bellerby, R., Wong, C. S., Delille, B., Bates, N. R., and de Baar, H. J. W.: Climatological mean and decadal change in surface ocean pCO_2, and net sea–air CO_2 flux over the global oceans, Deep Sea Research Part II: Topical Studies in Oceanography, 56, 554-577, doi:10.1016/j.dsr2.2008.12.009, 2009.

Treydte, K., Frank, D., Esper, J., Andreu, L., Bednarz, Z., Berninger, F., Boettger, T., D'Alessandro, C. M., Etien, N., Filot, M., Grabner, M., Guillemin, M. T., Gutierrez, E., Haupt, M., Helle, G., Hilasvuori, E., Jungner, H., Kalela-Brundin, M., Krapiec, M., Leuenberger, M., Loader, N. J., Masson-Delmotte, V., Pazdur, A., Pawelczyk, S., Pierre, M., Planells, O., Pukiene, R., Reynolds-Henne, C. E., Rinne, K. T., Saracino, A., Saurer, M., Sonninen, E., Stievenard, M., Switsur, V. R., Szczepanek, M., Szychowska-Krapiec, E., Todaro, L., Waterhouse, J. S., Weigl, M., and Schleser, G. H.: Signal strength and climate calibration of a European tree-ring isotope network, Geophysical Research Letters, 34, doi:10.1029/2007gl031106, 2007.

Treydte, K., Boda, S., Graf Pannatier, E., Fonti, P., Frank, D., Ullrich, B., Saurer, M., Siegwolf, R., Battipaglia, G., Werner, W., and Gessler, A.: Seasonal transfer of oxygen isotopes from precipitation and soil to the tree ring: source water versus needle water enrichment, New Phytologist, 202, 772-783, doi:10.1111/nph.12741, 2014.

© Author(s) 2019. CC BY 4.0 License.

Turney, C. S. M., Palmer, J., Maslin, M. A., Hogg, A., Fogwill, C. J., Southon, J., Fenwick, P., Helle, G., Wilmshurst, J. M., McGlone, M., Bronk Ramsey, C., Thomas, Z., Lipson, M., Beaven, B., Jones, R. T., Andrews, O., and Hua, Q.: Global Peak in Atmospheric Radiocarbon Provides a Potential Definition for the Onset of the Anthropocene Epoch in 1965, Scientific Reports, 8, doi:10.1038/s41598-018-20970-5, 2018.

van der Sleen, P., Groenendijk, P., and Zuidema, P. A.: Tree-ring delta O-18 in African mahogany (*Entandrophragma utile*) records regional precipitation and can be used for climate reconstructions, Global and Planetary Change, 127, 58-66, doi:10.1016/j.gloplacha.2015.01.014, 2015.

van der Sleen, P., Zuidema, P. A., and Pons, T. L.: Stable isotopes in tropical tree rings: theory, methods and applications, Functional Ecology, 31, 1674-1689, doi:f10.1111/1365-2435.12889, 2017.

Vicente-Serrano, S. M., Beguería, S., and López-Moreno, J. I.: A multiscalar drought index sensitive to global warming: the standardized precipitation evapotranspiration index, Journal of Climate, 23, 1696-1718, 2010a.

Vicente-Serrano, S. M., Beguería, S., López-Moreno, J. I., Angulo, M., and El Kenawy, A.: A new global 0.5 gridded dataset (1901–2006) of a multiscalar drought index: comparison with current drought index datasets based on the Palmer Drought Severity Index, Journal of Hydrometeorology, 11, 1033-1043, 2010b.

Vicente-Serrano, S. M., Van der Schrier, G., Beguería, S., Azorin-Molina, C., and Lopez-Moreno, J.-I.: Contribution of precipitation and reference evapotranspiration to drought indices under different climates, Journal of Hydrology, 526, 42-54, 2015.

Wacker, L., Bonani, G., Friedrich, M., Hajdas, I., Kromer, B., Němec, M., Ruff, M., Suter, M., Synal, H., and Vockenhuber, C.: MICADAS: routine and high-precision radiocarbon dating, Radiocarbon, 52, 252-262, 2010a.

Wacker, L., Němec, M., and Bourquin, J.: A revolutionary graphitisation system: Fully automated, compact and simple, Nuclear Instruments and Methods in Physics Research Section B: Beam Interactions with Materials and Atoms, 268, 931-934, doi:10.1016/j.nimb.2009.10.067, 2010b.

Walters, K. R., and Sjoberg, W. F.: The Persian Gulf Region. A Climatological Study, Air Force Environmental Technical Applications Center Scott AFB,IL. Technical Note. Accession Number: ADA222654, 1-73, 1990.

White, J.W.C., B.H. Vaughn, and S.E. Michel.: Stable Isotopic Composition of Atmospheric Carbon Dioxide (13C and 18O) from the NOAA ESRL Carbon Cycle Cooperative Global Air Sampling Network, 1990-2014, Version: 2015-10-26, ftp://aftp.cmdl.noaa.gov/data/trace_gases/co2c13/flask/. University of Colorado, Institute of Arctic and Alpine Research (INSTAAR), 2015.

Wickens, G. E.: The uses of the baobab (*Adansonia digitata* L.) in Africa, in: Browse in Africa: The current state of knowledge, edited by: Le Houérou, H. N., International Livestock Centre for Africa, Addis Ababa, 1979.

Wickens, G. E., and Lowe, P.: The Baobabs: Pachycauls of Africa, Madagascar and Australia, Springer Verlag, London, UK, 2008.

https://doi.org/10.5194/bg-2019-325
Preprint. Discussion started: 26 August 2019
© Author(s) 2019. CC BY 4.0 License.

Wieloch, T., Helle, G., Heinrich, I., Voigt, M., and Schyma, P.: A novel device for batch-wise isolation of α-cellulose from small-amount wholewood samples, Dendrochronologia, 29, 115-117, doi:10.1016/j.dendro.2010.08.008, 2011.

Woodborne, S., Hall, G., Robertson, I., Patrut, A., Rouault, M., Loader, N. J., and Hofmeyr, M.: A 1000-Year Carbon Isotope Rainfall Proxy Record from South African Baobab Trees (*Adansonia digitata* L.), PLoS ONE, 10, e0124202, 10.1371/journal.pone.0124202, 2015.

Woodborne, S., Gandiwa, P., Hall, G., Patrut, A., and Finch, J.: A Regional Stable Carbon Isotope Dendro-Climatology from the South African Summer Rainfall Area, PLoS ONE, 11, e0159361, 10.1371/journal.pone.0159361, 2016.

Woodborne, S., Hall, G., Jones, C. W., Loader, N. J., Patrut, A., Patrut, R. T., Robertson, I., Winkler, S. R., and Winterbach, C. W.: A 250-year isotopic proxy rainfall record from southern Botswana, Stud. Univ. Babes-Bolyai Chem., 63, 109-123, doi:10.24193/subbchem.2018.1.09, 2018.

Wushiki, H.: $^{18}O/^{16}O$ and D/H of the Meteoric Waters in South Arabia, Mass Spectrometry 39, 239-250, 1991.

Xu, C. X., Sano, M., Yoshimura, K., and Nakatsuka, T.: Oxygen isotopes as a valuable tool for measuring annual growth in tropical trees that lack distinct annual rings, Geochemical Journal, 48, 371-378, doi:10.2343/geochemj.2.0312, 2014.

https://doi.org/10.5194/bg-2019-325
Preprint. Discussion started: 26 August 2019
© Author(s) 2019. CC BY 4.0 License.

Biogeosciences Discussions Open Access EGU

Tables and Figures

Table 1: Compilation of published oxygen stable isotope data of monsoon rainfall, fog, stemflow, throughfall, and cyclone water from the Dhofar mountains for different years. Site coordinates are as follows: Salalah (17° 01' N, 54° 04' E), Qairoon Hairitti (17° 15' N, 54° 05' E), Gogub (17° 12' N, 54° 06' E), Tawi Atir (17° 06' N, 54° 31' E), Qarhanout (17° 07' N, 54° 37' E).

Year	Sampling period	type	$\delta^{18}O$ ‰ VSMOW	sd	n	Site	Altitude m asl	Reference
1988	06/01-08/12	rainfall	0.16	0.37	30	Salalah	20	Wushiki, 1991
1989	06/03-05/08	rainfall	0.31	0.57	25	Salalah	20	Wushiki, 1991
1989	07/01-08/08	rainfall	-0.52	0.26	42	Qairoon Hairitti	880	Wushiki, 1991
2008	Jun-Aug	rainfall	0.03	0.02	2	Gogub	450	Strauch et al., 2014
2009	Aug	rainfall	-0.22	0.07	4	Gogub	450	Strauch et al., 2014
Average		rainfall	-0.05	0.26	103			
2009	08/17-08/19	fog	0.09	0.08	3	Gogub	450	Strauch et al., 2014
2009	08/18-08/20	fog	-0.08	0.16	2	Tawi Atir	650	Strauch et al., 2014
Average		fog	0.01	0.12	5			
2009	08/17-08/19	throughfall	0,02	0,02	3	Gogub	450	Strauch et al., 2014
2009	08/18-08/20	throughfall	-0.01	0.25	2	Tawi Atir	650	Strauch et al., 2014
2011	08/09-08/11	throughfall	0.04	0.32	8	Tawi Atir	650	Strauch et al., 2014
Average		throughfall	0.02	0.20	13			
2009	08/17-08/19	stemflow	0.09	0.07	3	Gogub	450	Strauch et al., 2014
2009	08/18-08/20	stemflow	0.03	0.24	2	Tawi Atir	650	Strauch et al., 2014
Average		stemflow	0.06	0.16	5			
1988	Apr	cyclone	-2.79		1	Salalah	20	Wushiki, 1991
2011	11/04	cyclone	-10.76		1	Qarhanout near Jabal Samhan	~ 940	Strauch et al., 2014

https://doi.org/10.5194/bg-2019-325
Preprint. Discussion started: 26 August 2019
© Author(s) 2019. CC BY 4.0 License.

Biogeosciences Discussions Open Access EGU

820 **Table 2: Comparison of the $F^{14}C$ values of terminal parenchyma bands (TPBs) and the corresponding tree ring (TR). In case of multiple measurements per ring, the mean value was taken for comparison. Considering the youngest possible calibrated age, most TPBs are significantly younger than the corresponding tree ring. End of growth assumed to be end of September, i.e. at 0.75 of each year. Please note that the calibration always yields age ranges on the rising side of the bomb peak as well as on the falling part. For years < 1964 only the rising side and for years > 1965 only the falling side was considered for consistency. Underlined calibrated ages are viable, others are theoretical, only, and given for sake of completeness.**

Sample ID	Year of wood formation	$F^{14}C_{TB}$	(mean) $F^{14}C_{TR}$	difference TB-TR (%)	TB ages calibrated with SH1-2 (95.4 %)	TB ages calibrated with NH3 (95.4 %)
242.PB	1960	1.281780	1.227284	4.4	(6.1 %) 1962.6 AD to 1962.96 AD (4.8 %) 1963.18 AD to 1963.42 AD (4.7 %) 1979.6 AD to 1979.88 AD (76.6 %) 1980.12 AD to 1981.34 AD (3.2 %) 1982 AD to 1982.2 AD	(5.7 %) 1962.34 AD to 1962.64 AD (89.7 %) 1979.3 AD 1980.7 AD
237.PB	1961	1.381735	1.286768	7.4	(35.5 %) 1963.52 AD to 1964.08 AD (59.9 %) 1975.2 AD to 1976.12 AD	(9.8 %) 1962.76 AD to 1963.12 AD (85.6 %) 1974.74 AD to 1976.08 AD
231.PB	1962	1.349989	1.266081	6.6	(13.7 %) 1963.34 AD to 1963.76 AD (81.7 %) 1976.3 AD to 1977.48 AD	(6.2 %) 1962.58 AD to 1963 AD (89.2 %) 1976.1 AD to 1977.66 AD
223.PB	1963	1.460845	1.414688	3.3	(7.3 %) 1964 AD to 1964.2 AD (88.1 %) 1972.48 AD to 1973.38 AD	(8.7 %) 1962.98 AD to 1963.4 AD (72.2 %) 1972.16 AD to 1973.06 AD (14.5 %) 1973.28 AD to 1973.96 AD
19.PB	2005	1.056946	1.061611	-0.4	(5.0 %) 1957.6 AD to 1958.08 AD (90.4 %) 2008.18 AD to 2011.1 AD	(2.3 %) 1957.62 AD to 1967.88 AD (1.2 %) 2006.22 AD to 2006.36 AD (91.9 %) 2006.84 AD to …

825

https://doi.org/10.5194/bg-2019-325
Preprint. Discussion started: 26 August 2019
© Author(s) 2019. CC BY 4.0 License.

Biogeosciences Discussions Open Access EGU

Table 3: Significant correlations between the obtained baobab time series and climate parameters for the area around Wadi Hinna. Correlations within months of the current year are marked by upper case abbreviations, correlations within months of the previous year by lower case abbreviations and a grey background. Significance levels: * $p < 0.05$, ** $p < 0.01$, *** $p < 0.001$, **** $p < 0.0001$. Positive (negative) correlations are indicated with "+" ("-"). Note: $\delta^{13}C$ vales show some significant but weak correlations compared to RWI and $\delta^{18}O$.

Baobab/ climate parameter	RWI	$\delta^{13}C^{*}_{min}$	$\delta^{13}C^{*}_{mean}$	$\delta^{13}C^{*}_{max}$	$\delta^{18}O_{min}$	$\delta^{18}O_{mean}$	$\delta^{18}O_{max}$
precipitation	apr*- jul*- jan-dec*-	jan*-		oct*- jan-dec*-			jan-dec*-
	May**+ Aug***+ May-Sep***+ Jan-Dec*+	Nov**+			Apr*- May****- May-Sep**- Jan-Dec**-	Apr*- May****- May-Sep***- Jan-Dec***-	
T_{max}				oct*-	dec*-		
	Sep/Oct*-		May*-	May*-	Feb/Mar*-		
vapor pressure				jan-dec*- feb/mar/apr*- oct*-			feb*-
			Mar*- May*-	May*-	Feb/Mar*-		
cloud cover							oct*-
				Apr*-	Feb*-	Apr*-	Apr***- Aug**-
rH anomality			aug*+		jan*+ jul/aug**+	jul*+ aug**+	nov*+
					Mar*+	Mar*+	Mar*+
SPEI (1 month)	oct*- dec**+		nov*+		apr*+ dec*-	dec**-	
	Jan*+ May*+ Aug**+ May-Sep*+ Jan-Dec*+		Nov*+	May*+ Nov*+	May**- Aug**- May-Sep*-	May**- Aug*- May-Sep*-	Oct*+

https://doi.org/10.5194/bg-2019-325
Preprint. Discussion started: 26 August 2019
© Author(s) 2019. CC BY 4.0 License.

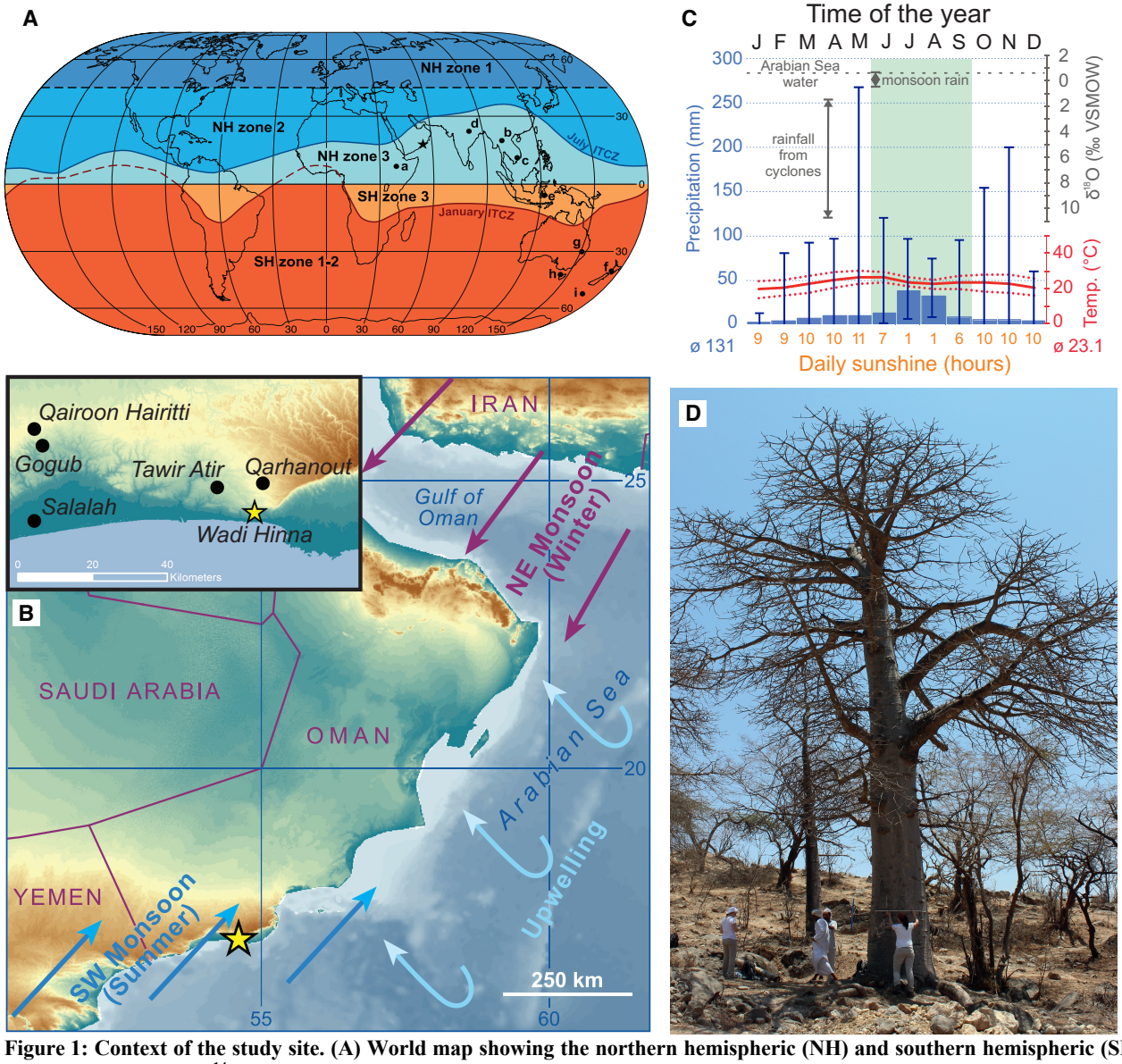

Figure 1: Context of the study site. (A) World map showing the northern hemispheric (NH) and southern hemispheric (SH) zones of atmospheric bomb ^{14}C (after Hua, et al. 2013). Zones close to the equator (NH3, SH3) are still underrepresented in studies reconstructing the atmospheric radiocarbon content. Star indicates study site; sites labeled with letters a-i correspond to sample locations of $F^{14}C$ studies referred to in figure 5. (B) Map showing the location (yellow star) of the tree site Wadi Hinna (318 m asl) at the edge of the Dhofar mountains in southern Oman (17° 03' N, 54° 36' E) (map topography based on SRTM and bathymetry data from Becker et al. 2009). Prevailing seasonal wind patterns are shown by blue (summer monsoon, rainfall season) and purple arrows (winter monsoon, dry season). Light blue arrows indicate upwelling of deep waters from the Arabian Sea. (C) Climate diagram for the area around Wadi Hinna (17.0-17.5° N, 54.0-54.5° S) with average mean precipitation (bars indicating minima and maxima; source: GPCC, gpcc_V7_05) and temperature for 1942-2013 (dotted lines representing Tmin and Tmax, respectively; source: CRU TS4.01, GPCC V7_05). The isotopic signature of the Arabian Sea water and the precipitation around the study site is indicated in dark grey and varies significantly between monsoonal and non-monsoonal precipitation (Wushiki, 1991; Strauch et al., 2014). Average daily sunshine hours are given in orange (1979-1990, NOAA: ftp://ftp.atdd.noaa.gov/pub/GCOS/WMO-Normals/RA-II/OM/41316.TXT) and the timing of the summer monsoon and the approximate growing season of the baobab trees is indicated in green. (D) Sampled baobab tree at Wadi Hinna.

https://doi.org/10.5194/bg-2019-325
Preprint. Discussion started: 26 August 2019
© Author(s) 2019. CC BY 4.0 License.

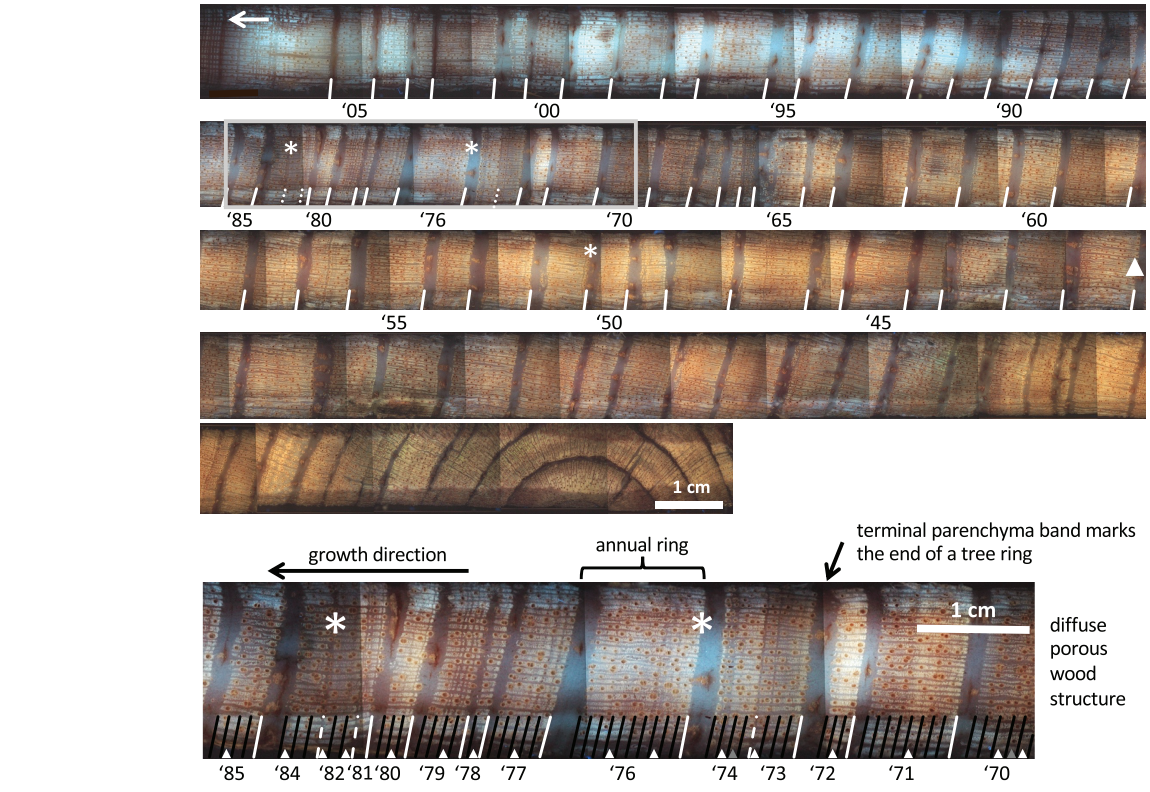

Figure 2: Wood anatomy of the sampled baobab core. The right side of each photograph is unintentionally darker, causing vertical cut-offs in the stitched panorama. Asterisks mark positions of missing rings. Top: Stitched core picture photographed under ultra-violet light with automatic white balance showing alternating diffuse porous wood sections and clearly defined terminal parenchyma bands. Tree-ring boundaries and years of growth are indicated for the analyzed core section, i.e. from cambium (white arrow, top left) until 1941 (white triangle). Bottom: Enlarged core section (grey frame on top) with indicated tree-ring boundaries (white lines), subsamples (black lines), dated samples (white triangles: hemicellulose, grey triangles: alpha cellulose) and years of growth. Boundaries indicated by dashed white lines were only identified after intensified ^{14}C dating.

https://doi.org/10.5194/bg-2019-325
Preprint. Discussion started: 26 August 2019
© Author(s) 2019. CC BY 4.0 License.

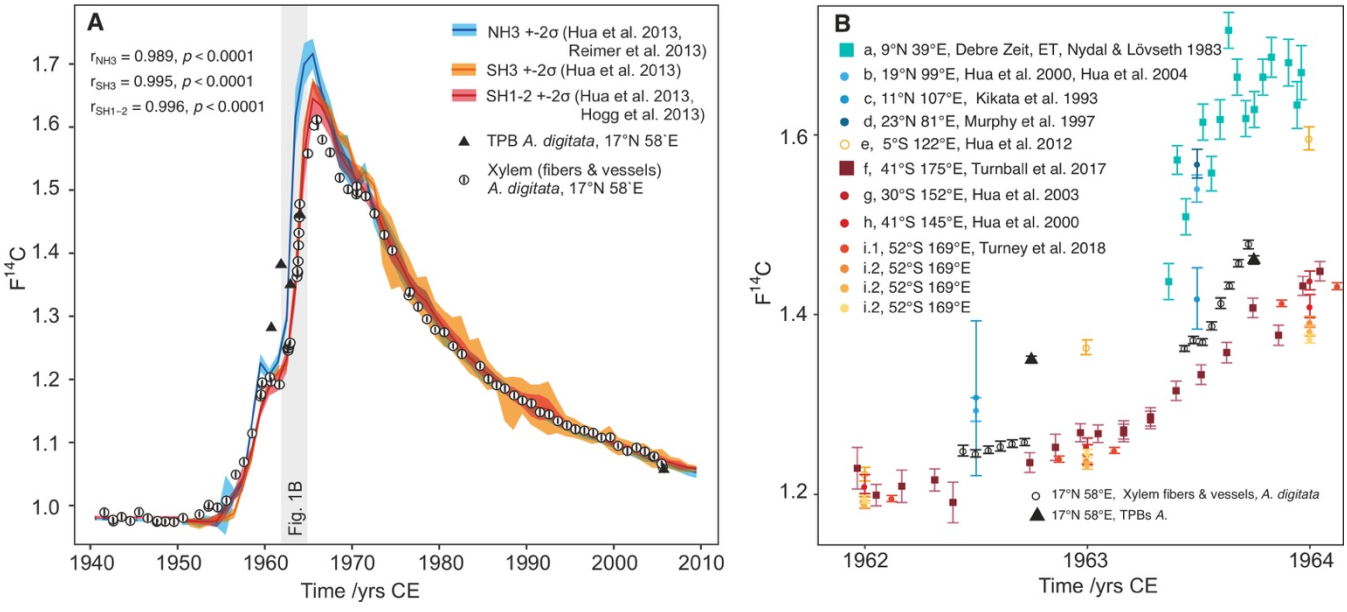

Figure 3: (A) Comparison of baobab $F^{14}C$ values with $F^{14}C$ curves for both hemispheres. Data prior to 1950 taken from IntCal13 and SHCal13 (Reimer et al., 2013, Hogg et al., 2013). 1950-2010 originates from Hua et al., 2013 (line: mean value, shade: ± 2 standard deviations (σ)). The southern hemispheric increase in atmospheric $F^{14}C$ lags behind the northern hemisphere by about 1 year and its peak is considerably shallower. The overall conformity of the baobab measurements (white dots with 2 σ error bar) with the course of the calibration curves proves the annual character of the growth zones. The values for baobab tree-ring cellulose (xylem fibers and vessels) lie between the values for both hemispheres for the steep increase in $F^{14}C$ and then apparently follow the course of SH1-2, although temporary shifted due to different vegetation periods. Four out of five terminal parenchyma bands (TPB, black triangles, error bars are smaller than the symbol size) show either much higher $F^{14}C$ values (1960-1962) or a lower value (2005) than the corresponding tree ring. (B) Baobab measurements in comparison to atmospheric (squares) and tree-ring data (circles) for NH3 (a-d), SH3 (e), and SH1-2 (f-i) between 1962 and 1964. These years show strongly increasing atmospheric $F^{14}C$ values and were chosen to investigate the intra-annual baobab $F^{14}C$ values. For this period, the baobab $F^{14}C$ values lie between the higher NH3/SH3 and the lower SH1-2 values. A dip within the first half of the tree ring is followed by a slight (1962) or steep (1963) increase of the values. Note, the inter- and intra-species' variability from the same site (i.1 and i.2, Turney et al., 2018).

https://doi.org/10.5194/bg-2019-325
Preprint. Discussion started: 26 August 2019
© Author(s) 2019. CC BY 4.0 License.

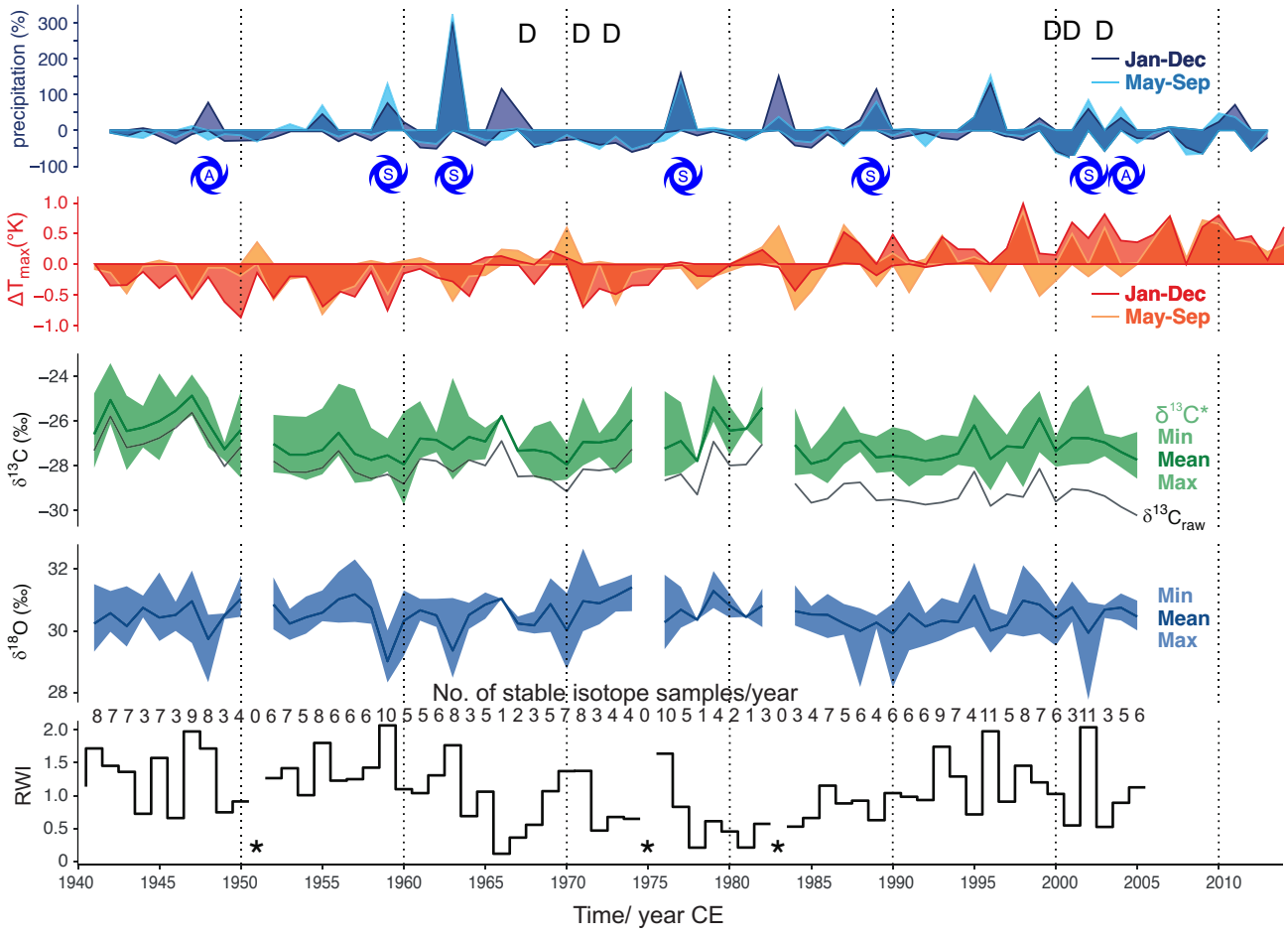

Figure 4: Analyzed baobab tree-ring parameters (ring width indices (RWI), $\delta^{18}O$, $\delta^{13}C^*$) together with available precipitation and T_{max} data for the period 1941-2014. Precipitation is presented as percentage differences from the mean, T_{max} as differences in Kelvin. Darker colors reflect differences on an annual basis, lighter colors for the monsoon period Jun-September. The stable isotope values ($\delta^{13}C^*$, $\delta^{18}O$) are presented with minima, maxima and mean values for each year. Mean δ13C, uncorrected for effects of changing atmospheric CO_2 concentration and corresponding $\delta^{13}C_{CO2}$ is given as black line ($\delta^{13}C_{raw}$). Dry years with ≤ 45 mm of rain during the monsoon period are marked with D. Years with spring (S) or autumn (A) storms with ≥ 90 mm of rain are indicated by cyclone symbols. Missing rings caused gaps in the time series and are marked by asterisks.

https://doi.org/10.5194/bg-2019-325
Preprint. Discussion started: 26 August 2019
© Author(s) 2019. CC BY 4.0 License.

Biogeosciences Discussions
Open Access
EGU

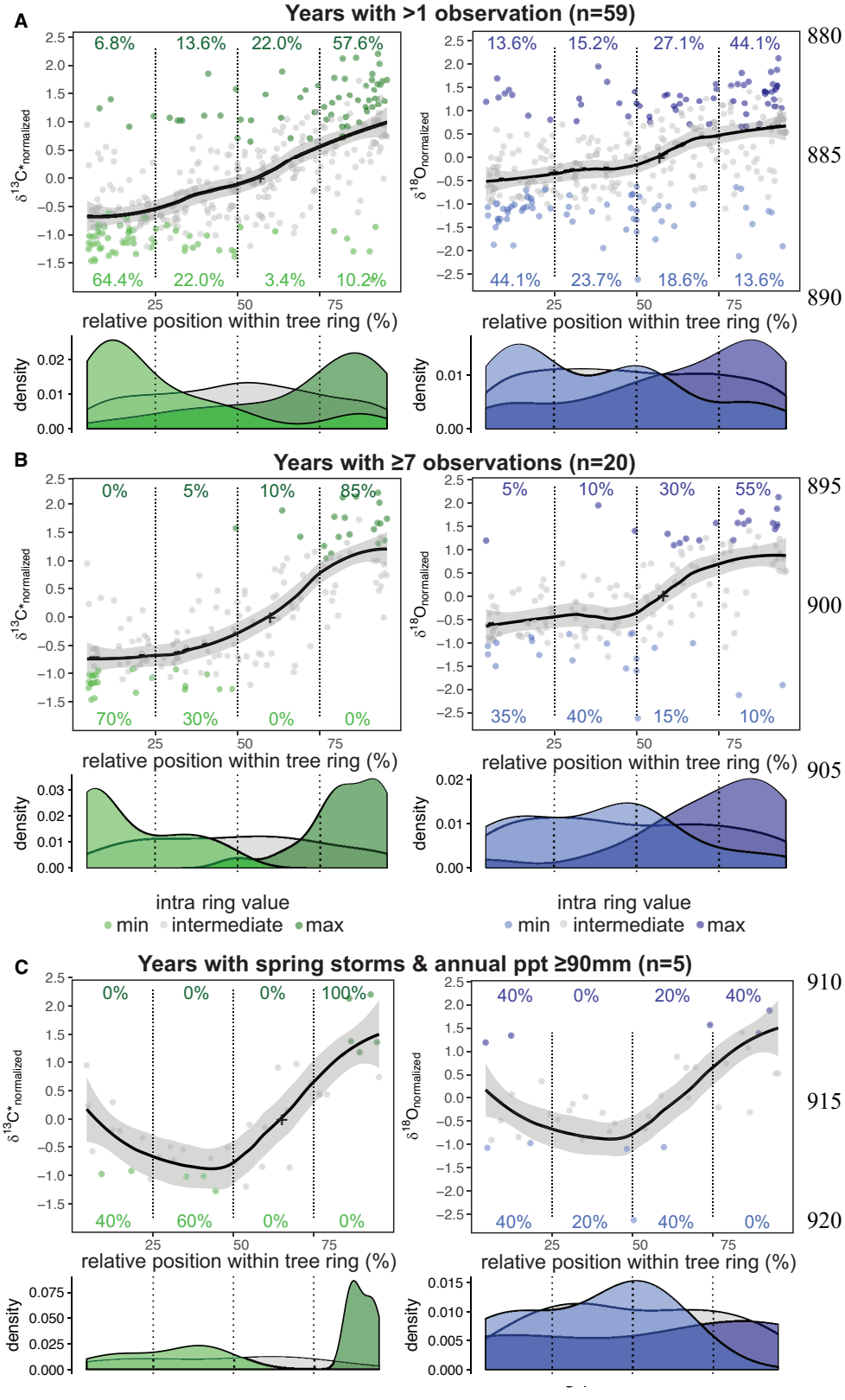

Figure 5: Relative position of normalized $\delta^{13}C^*$ (green) and $\delta 18O$ (blue) values (A-C). Smooth line illustrates the intra-annual course of the isotope ratios with the standard error as grey shaded area (loess fit with span = 0.6).

(A) For both $\delta^{13}C^*$ and $\delta^{18}O$ the first half of the tree ring is dominated by minimum values, the second half by maximum values.

(B) The common isotopic pattern becomes clearer for tree rings ≥ 7 samples. $\delta^{13}C^*$ shows a gentle increase during the first two quarters, then increases strongly, before levelling off in the last quarter. $\delta^{18}O$ is characterized by a dip in the mid-section before the steep rise of the values.

(C) For years with spring cyclones ≥ 90 mm of rain (i.e. average monsoon precipitation (ppt); ≥ 5 observations per year; n = 5; 1959, 1963, 1977, 1989, 2002), $\delta^{13}C^*$ shows decreasing values within the first half of the tree ring and a steep increase in the second half. The $\delta^{18}O$ values show their minimum at the center of the tree ring, followed by a steep rise towards the end of the tree ring.

https://doi.org/10.5194/bg-2019-325
Preprint. Discussion started: 26 August 2019
© Author(s) 2019. CC BY 4.0 License.

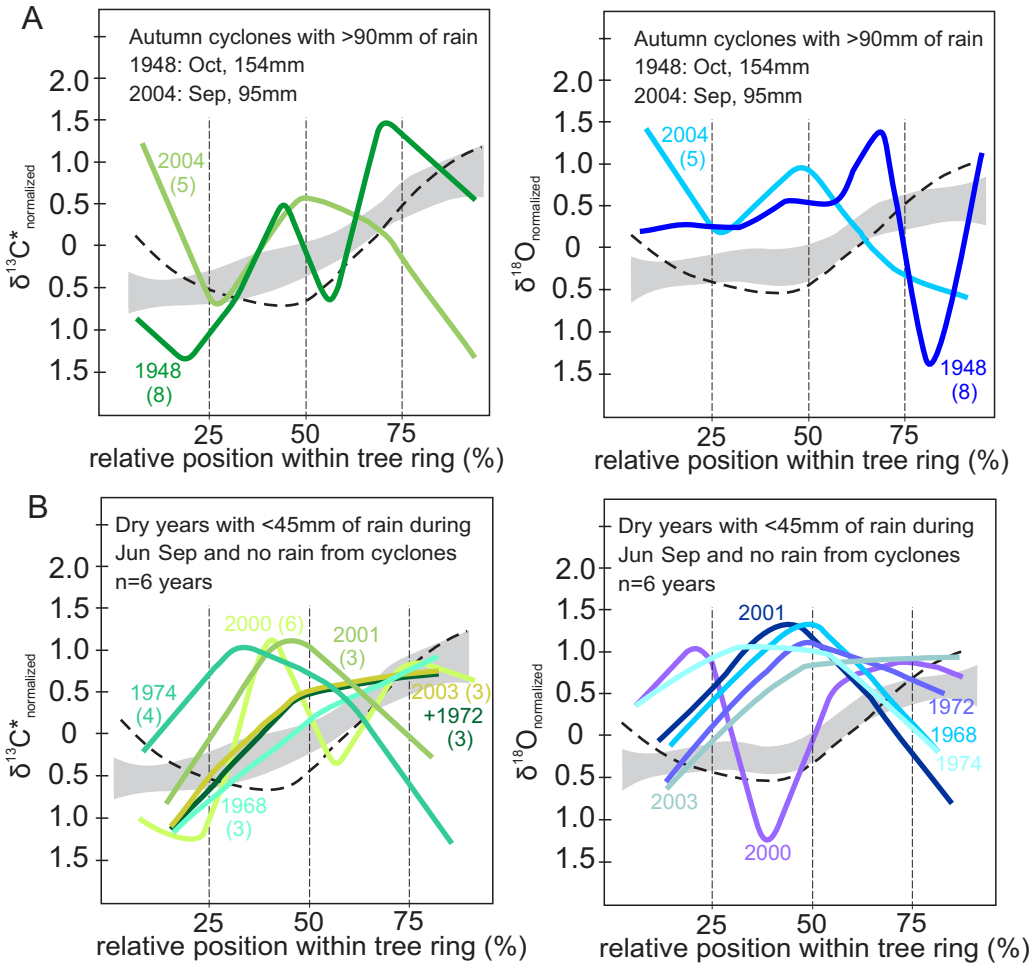

Figure 6: (A) Intra-annual course of normalized $\delta^{13}C^*$ (green) and $\delta^{18}O$ (blue) values for years with autumn cyclones bringing ≥ 90 mm of rain (n = 2) and (B) dry years with ≤ 45 mm monsoonal precipitation and no rain from cyclones (n = 6). Numbers in brackets indicate number of isotope samples analyzed per year. Grey shaded area marks intra-annual course of isotope ratios with standard error for all years with ≥ 3 observations. Dashed line indicates intra-annual course of isotopes for years with spring cyclones, illustrated in detail in Fig. 5C. Rain from autumn cyclones may affect the intra-annual isotope signature by more strongly declining values towards the end of a tree ring. Years with less than 45 mm of monsoon precipitation show an increase in $\delta^{13}C^*$ towards the middle of each tree ring, then decline or increase only slightly towards the end. Rather similar seasonal trends can be observed for $\delta^{18}O$ values. Hence, dry monsoon seasons usually cause higher isotope values in the middle part of each tree ring than during normal years. Please see text for further details on the conspicuous seasonal trends in 1948 and 2000.

https://doi.org/10.5194/bg-2019-325
Preprint. Discussion started: 26 August 2019
© Author(s) 2019. CC BY 4.0 License.

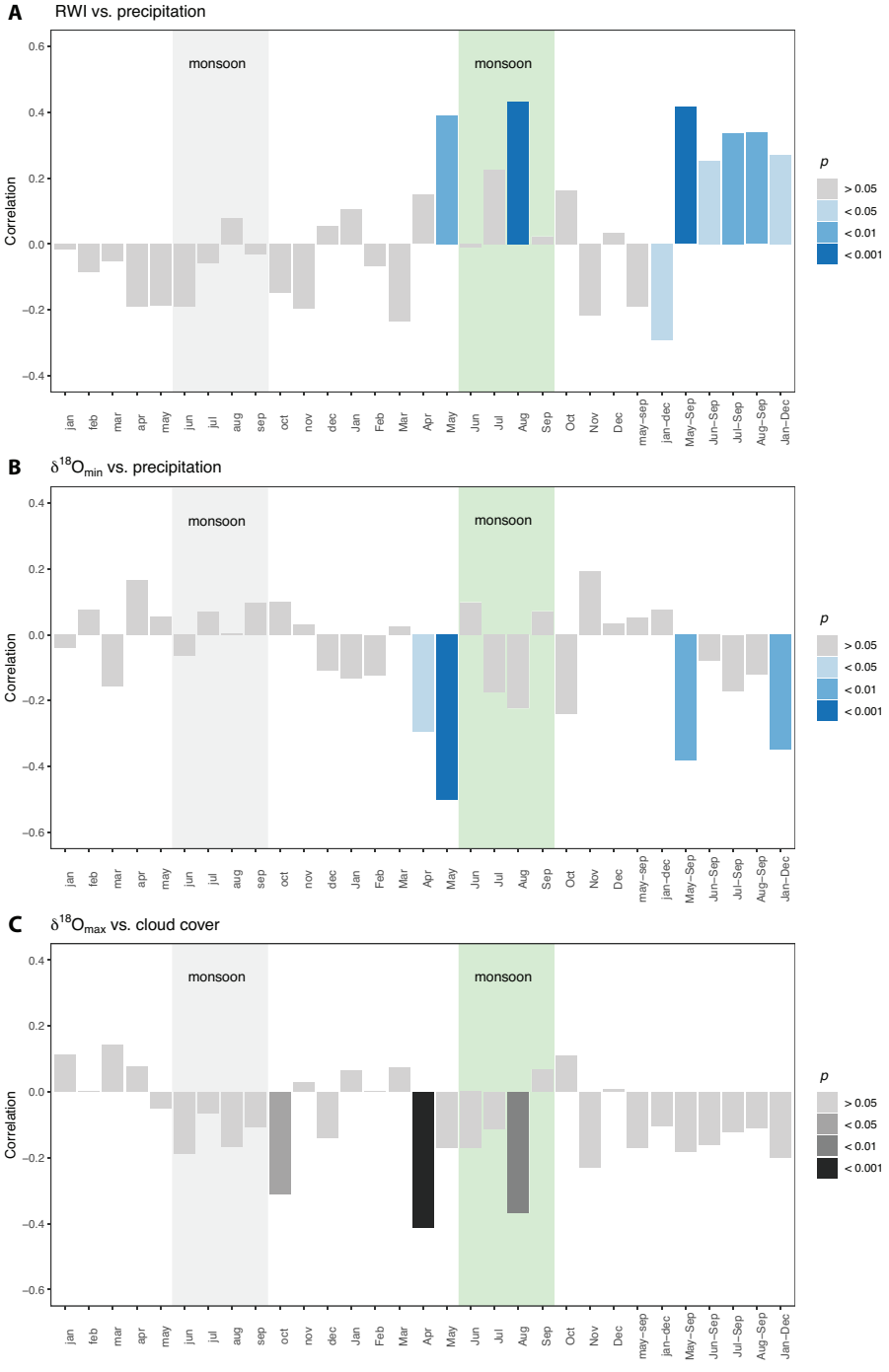

Figure 7: Diagrams for the strongest correlations of baobab tree-ring parameters with monthly and seasonally resolved climate parameters. Months of the previous year are marked by lower case abbreviations, months of the current year by upper case abbreviations. The green box marks the average monsoon period. (A) Ring-width indices versus precipitation amount. (B) δ^{18}Omin versus precipitation. (C) δ^{18}Omax versus cloud cover. Apart from the actual monsoon season (Jun-Sep) also the pre-monsoon (Apr-May) has a significant influence on wood increment growth and δ^{18}O isotope signature.

https://doi.org/10.5194/bg-2019-325
Preprint. Discussion started: 26 August 2019
© Author(s) 2019. CC BY 4.0 License.

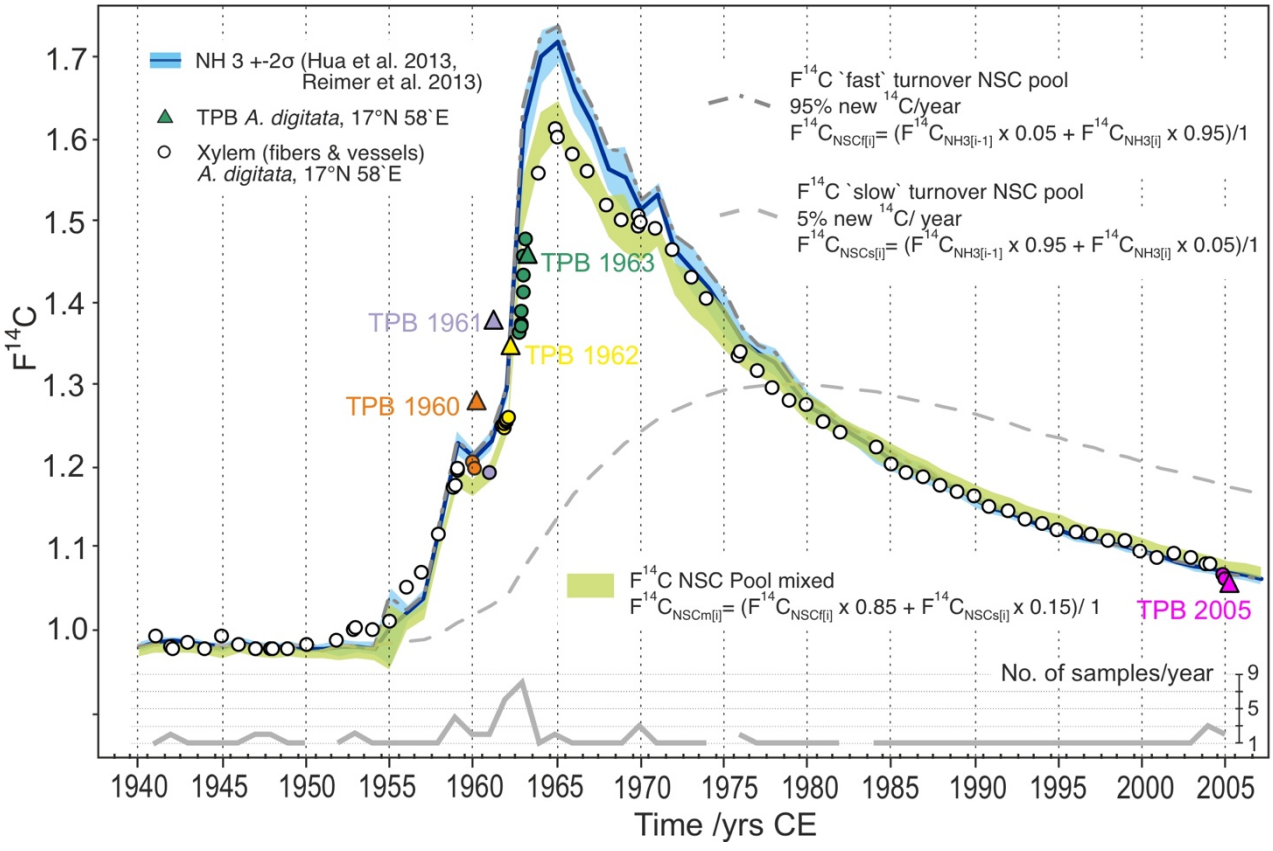

Figure 8: Baobab $F^{14}C$ values in comparison with the $F^{14}C$ curve for NH3 (blue line/shade) and modelled pools of non-structural carbohydrates (NSC) fueling wood formation. The observed $F^{14}C$ values of baobab xylem fibers and vessels (circles) are well approximated by assuming polymerization from a mixed NSC pool ($F^{14}C_{NSCm[i]}$) with contributions from a fast ($F^{14}C_{NSCf[i]}$) and slow ($F^{14}C_{NSCs[i]}$) turnover NSC pool, respectively. Range of $F^{14}C_{NSCm[i]}$ (green shade) is given by the 2σ range of atmospheric $F^{14}C$ source values ($F^{14}C_{NH3[i]}$) for each year ($_{[i]}$). 1940 was chosen as starting year for the model calculations. Terminal parenchyma bands (TPB, colored triangles) show higher (1960-1962) and lower (2005) $F^{14}C$ values than $F^{14}C$ of NH3 and xylem fibre and vessel tissue of corresponding tree rings. This indicates distinct younger ages of TPBs and points to structural changes and ongoing cell division of parenchyma tissue for a number of years after initial formation. Some $F^{14}C$ values of fiber and vessel samples (e.g. 1945, 1953, 1954, 1957, 1958) were also found above corresponding NH3 values. This might allude to the presence of intraxylary parenchyma tissue that could not be detected during the tree-ring dissection process.